Using flow cytometry and light-induced fluorescence technique to characterize the variability and characteristics of bioaerosols in springtime at Metro Atlanta, Georgia

Arnaldo Negron[a,b], Natasha DeLeon-Rodriguez[c$], Samantha M. Waters[a#], Luke D. Ziemba[d], Bruce Anderson[d], Michael Bergin[e], Konstantinos T. Konstantinidis[f,c*], and Athanasios Nenes[a,~~b,~~g,h,~~i~~*]

[a] School of Earth and Atmospheric Sciences, Georgia Institute of Technology, Atlanta, GA 30332, USA
[b] School of Chemical and Biomolecular Engineering, Georgia Institute of Technology, Atlanta, GA 30332, USA
[c] School of Biology, Georgia Institute of Technology, Atlanta, GA 30332, USA
[d] Chemistry and Dynamics Branch/Science Directorate, National Aeronautics and Space Administration Langley Research Center, Hampton, VA 23681, USA
[e] Department of Civil and Environmental Engineering, Duke University, Durham, NC, 2770, USA
[f] School of Civil and Environmental Engineering, Georgia Institute of Technology, Atlanta, GA 30332, USA
[g] Institute ~~of Environmental Research & Sustainable Development, National Observatory of Athens, GR-15236, Greece~~
[h] ~~Institute~~ for Chemical Engineering Science, Foundation for Research and Technology Hellas, Patra, GR-26504, Greece
[~~i~~h] Laboratory of Atmospheric Processes and their Impacts (LAPI), School of Architecture, Civil & Environmental Engineering, Ecole Polytechnique Fédérale de Lausanne, CH-1015, Switzerland
[$] Currently at: Puerto Rico Science, Technology and Research Trust, Rio Piedras, 00927, Puerto Rico
[#] Currently at: Department of Marine Sciences, University of Georgia, Athens, GA 30602-3636
*Corresponding Author

Abstract

The abundance and speciation of primary biological aerosol particles (PBAP) is important for understanding their impacts on human health, cloud formation and ecosystems. Towards this, we have developed a protocol for quantifying PBAP collected from large volumes of air with a portable wet-walled cyclone bioaerosol sampler. A flow cytometry (FCM) protocol was then developed to quantify and characterize the PBAP populations from the sampler, which were confirmed against epifluorescence microscopy. The sampling system and FCM analysis were used to study PBAP in Atlanta, GA over a two-month period and showed clearly defined populations of DNA-containing particles: Low Nucleic Acid-content particles ~~(bioLNA),~~above threshold (LNA-AT), and High Nucleic Acid-content particles (HNA) ~~being~~likely containing wet-ejected fungal spores and pollen. We find that daily-average springtime PBAP concentration (1 to 5µm diameter) ranged between 1.4×10^4 and 1.1×10^5 m^{-3}. The ~~BioLNA~~LNA-AT

population dominated PBAP during dry days (72 ± 18%); HNA dominated the PBAP during humid days and following rain events, where HNA ~~(e.g., wet-ejected fungal spores)~~ comprised up to 92% of the PBAP number. Concurrent measurements with a Wideband Integrated Bioaerosol Sensor (WIBS-4A) showed that FBAP and total FCM counts are similar; HNA (from FCM) ~~significantly~~moderately correlated with ABC type FBAP concentrations throughout the sampling period (and for the same particle size range, 1-5 µm diameter). However, the FCM ~~bioLNA~~LNA-AT population, possibly containing bacterial cells, did not correlate ~~to~~with any FBAP type. The lack of correlation of any WIBS FBAP type with the ~~bioLNA~~LNA-AT suggest airborne bacterial cells may be more difficult to unambiguously detect with autofluorescence than ~~previously~~currently thought. ~~Identification~~Identification of bacterial cells even in the FCM (~~bioLNA~~LNA-AT population) is challenging, given that the fluorescence level of stained cells at times may be comparable to that seen from abiotic particles. HNA and ABC displayed highest concentration on a humid and warm day after a rain event (4/14), suggesting that both populations correspond to wet-ejected fungal spores. Overall, information from both instruments combined reveals a highly dynamic airborne bioaerosol community over Atlanta, with a considerable presence of fungal spores during humid days, and ~~a bioLNA~~LNA-AT population dominating bioaerosol community during dry days.

Introduction

Primary biological ~~atmospheric~~aerosol particles (PBAP), also called bioaerosols, are comprised of airborne microbial cells (e.g. bacteria, diatoms), reproductive entities (e.g. pollen, fungal spores), viruses and biological fragments. Bioaerosols are ubiquitous, with potentially important impacts on human health, cloud formation, precipitation, and biogeochemical cycles. (Pöschl, 2005; Hoose et al., 2010; DeLeon-Rodriguez et al., 2013; Morris et al., 2014; Longo et al., 2014; Fröhlich-Nowoisky et al., 2016; Myriokefalitakis et al., 2016). Despite their low number concentration relative to abiotic particles, PBAP possess unique functional and compositional characteristics that differentiate them from abiotic aerosol. For example, certain PBAP constitute the most efficient of atmospheric ice nucleators, affecting the microphysics of mixed phase clouds and precipitation (Hoose and Möhler, 2012; Sullivan et al., ~~2018~~2017). The mass and nutrient content of PBAP may suffice to comprise an important supply of bioavailable P to oligotrophic marine ecosystems (Longo et al., 2014; Myriokefalitakis et al., 2016). In addition, the concurrence of disease outbreaks during dust storms has been attributed to pathogenic microbes attached to airborne dust that are subsequently inhaled (Griffin et al., 2003; Ortiz-Martinez et al., 2015; Goudie 2014).

Quantification of the concentration and size of PBAP is critical for understanding their environmental impacts. Measuring PBAP however poses a challenge for established microbiology tools, owing to their low atmospheric concentration (10^3 - 10^6 cells m^{-3} air; Fröhlich-Nowoisky et al., 2016) and wide diversity

of airborne particle types and sizes. For instance, only a fraction of microorganisms (an estimated 5%; Chi and Li et al., 2007) can be cultured, and cultivation cannot be used to quantify dead organisms, viruses or fragments, while most culture-independent methods are optimized for more abundant microbial populations. Epifluorescence microscopy (EPM) is the standard for bioaerosol quantification but is not high-throughput and requires considerable time for quantification of concentration per sample. Flow cytometry (FCM) is an analysis technique based on the concurrent measurement of light scattering and fluorescence intensity from single particles (Wang et al., 2010). FCM requires a liquid suspension of bioparticles that flows through an optical cell and interrogated with a series of laser beams. Each sample is pretreated with stains that targeting specific macromolecules (e.g. DNA/RNA) which subsequently fluoresce when excited by the FCM lasers. The resulting scattering and fluorescent light emissions are then detected by an array of sensors to allow the differentiation of biological and abiotic (e.g. dust) particles according to the characteristic specific to the stain used. FCM has proved to be as reliable as EPM, but with the advantage of lower uncertainty, higher quantification efficiency and requiring considerably less time and effort than EPM per sample (Lange et al., 1997). FCM is frequently used in biomedical research to quantify eukaryotic cell populations, and in microbiology to quantify a wide variety of yeast and bacterial cells (Nir et al., 1990; Van Dilla et al., 1983). FCM is also used to study environmental samples, e.g., to differentiate low nucleic acid (LNA) from high nucleic acid (HNA) phytoplankton in aquatic environments (Wang Y. et al 2010; Müller et al., 2010). Despite its advantages, FCM has seen little use in the bioaerosol field to date (e.g., Chen and Li, 2005; Liang et al., 2013), owing in part to the challenges associated with collecting sufficient PBAP mass for ~~sufficient~~robust counting statistics to be obtained (Chen and Li, 2005; Liang et al., 2013). Chen and Li (2005) determined that for counting purposes, the SYTO-13 nucleic acid stain is the most effective (among five different nucleic acid stains studied) for determining reliable concentration of bioaerosols.

~~The~~ SYTO-13 stain can also be used to provide insights on the stress/metabolic state of microbes. Guindulian et al. ~~(1997) used FCM to study biological particles in fresh and starved seawater samples collected from the West Mediterranean Sea (Spain). Samples were analyzed either immediately or after starvation for 2-3 days. Also, *E.coli* pure cultures were tested before and after starvation in sea water. In both situations, samples were treated with DNAse and RNAse and subsequently stained with SYTO-13 to measure cellular DNA content (starvation ensures that intracellular RNA is negligible in marine populations, so that the SYTO-13 intensity is directly related to the DNA content of cells). Guindulian et al.~~ (1997), with starved seawater samples and *E.coli* pure cultures together suggest that the stress level caused by marine starvation reduces RNA content in aquatic microorganisms to an undetectable level. This has important implications for the detection of atmospheric PBAP, as cells are exposed to multiple stressors when airborne.

Formatted: Font color: Text 1

Light Induced Fluorescence (LIF) is an increasingly utilized technique for bioaerosol quantification, and it relies on measuring the autofluorescence intensity of specific high yield fluorophores (e.g., Nicotinamide Adenine Dinucleotide – NADH co-enzyme, flavins and amino acids like Tryptophan and Tyrosine) present in PBAP. The major advantage of the technique is that it is fully automated, does not require a liquid suspension (i.e., it directly senses particles suspended in air) and ~~that~~it provides high frequency measurements (~1 Hz) ~~which~~ make it ideal for monitoring and ~~bioaerosol quantification.~~ operation in highly variable environments (e.g., aircraft operation). Particles detected by LIF, called Fluorescent Biological ~~Atmospheric~~Aerosol Particles (FBAP), although not equal to PBAP, may still constitute a large fraction of the biological particles (Healy et al., 2014; Gosselin et al., 2016). Using LIF, FBAP diurnal cycles showing maximum concentrations during evenings and minimum around middays, especially in heavily vegetated environments have been observed. This behavior has been related to known temperature and relative humidity release mechanism of certain fungal spore species (Wu et al., 2007; Gabey et al., 2010; Tropak and Schnaiter, 2013). Huffman et al. (2010) used a UV-Aerodynamic Particle Sizer (UV-APS) to show that the concentration and frequency of occurrence of 3µm FBAP particles at Mainz, Germany (semi-urban environment) exhibited a strong diurnal cycle from August through November: with a first peak at ~ 1.6×10^4 m^{-3} at mid-morning (6-8 am) followed by a constant profile (~ 2-4×10^4 m^3) throughout the rest of the day. Similar studies in urban and densely vegetated environments suggest a notable difference in the size distributions, diurnal behavior and FBAP loading between the two environments. Gabey et al., 2011 found that the FBAP in Manchester, UK follow a characteristic bimodal distribution with peaks at 1.2µm and 1.5 – 3.0 µm. As in Mainz, the concentration of larger particles peaks in the mid-morning, ranges from 0 to 300 L^{-1}, and the 1.2µm peak is linked to traffic activity. However, at the Borneo tropical rain forest FBAP concentrations peak during the evening with a robust 2-3µm population and concentrations ranging from 100 to 2000 L^{-1} (Gabey et al., 2010).

LIF-based observations (e.g. UV-APS, WIBS), combined with measurements of molecular tracers (e.g. mannitol and arabitol) and endotoxin measurements provide a more complete picture of PBAP emissions. Gosselin et al. (2016) applied this approach during the BEACHON-RoMBAS field campaign. A clear correlation between FBAP and the molecular markers is seen, indicating an increase of fungal spores during rain events. FBAP concentrations and molecular marker-inferred (arabitol and mannitol) fungal spore concentrations (1.7pg mannitol per spore and 1.2 pg arabitol per spore; Bauer et al., 2008) were within the same order of magnitude. The UV-APS FBAP concentration during rain events was higher than the fungal spore concentrations inferred from the concentration of molecular markers, which suggest other non-fungal spore fluorescent particles are detected as well as fungal spores by the UV-APS. In the same study, the WIBS-3 cluster (determined using Crawford et al., 2015) linked to fungal spores gave concentrations that were 13% lower than those derived from molecular marker concentrations during rain events. During dry

events, FBAP and molecular markers derived fungal spore concentrations were poorly correlated. It is currently unknown the degree to which all types of PBAP are consistently detected by LIF over different time of the year and different environments; it is likely, however, that for certain classes of bioparticles (e.g., pollen and fungi) the detection efficiency using LIF is relatively high. However, the low intrinsic fluorescence intensity of bacteria and high variability of thereof in relation to metabolic state may lead to their misclassification as non-biological particles (Hernandez et al., 2016).

For LIF-based quantification of PBAP to be effective, it requires the intrinsic fluorescence of biological material to exceed that of non-biological matter. Depending on the type, metabolic state and species, PBAP autofluorescence may vary orders of magnitude and therefore LIF may not always be able to differentiate between biological and abiotic particles. For example, Tropak and Schnaiter (2013) showed that laboratory-generated mineral dust, soot and ammonium sulfate may be misclassified as FBAP. To address misclassification, Excitation Emission Matrices (EEMs) have been developed for biomolecules (e.g. tryptophan, tyrosine, riboflavin) and non-biological (e.g. Pyrene, ~~Napthalane~~Naphthalene, Humic Acid) molecules. EEMs provide the wavelength-dependent fluorescence emission spectra as a function of the excitation wavelength and are used to assign spectral modes to known fluorophores. The structure of EEMs is important for identifying molecules that are unique to PBAP and allow their identification by LIF; it is this principle upon which detectors in commercial FBAP measurements (e.g. WIBS, UV-APS) are based upon. Comparison of EEMs from biological and non-biological molecules show that even when biomolecules have higher autofluorescence intensity than non-biologicals in the LIF detection range, interferences from non-biological compounds (e.g. polycyclic aromatic hydrocarbons and soot) from combustion emissions can influence LIF detection (Pöhlker et al., 2012). Considerable work remains on determining which detector(s) or combination thereof provides an unambiguous identification of bioaerosols and related subgroups (e.g. bacteria, fungal spores, pollen). Towards this, an aerobiology catalog of pure cultures has been developed for the WIBS-4 (Hernandez et al., 2016), where, (i) pollen and fungal spore species autofluoresce much more than bacteria, and, (ii) bioaerosol subgroups are more successfully discriminated by specific detector(s). However, the same study showed that instrument-to-instrument variability in fluorescence detection poses a considerable challenge, as applying common detection thresholds across instruments leads to considerable differences in PBAP concentration and composition.

Another important issue for LIF-based PBAP is the impact of atmospheric oxidants, UV and other stressors on the fluorescence intensity of PBAP. This is important, given the ~~prevalence~~ubiquity of PBAP throughout the atmosphere, including the extreme conditions in the upper troposphere (DeLeon-Rodriguez et al., 2013). Pan et al. (2014) tested the effect of relative humidity and ozone exposure in the

autofluorescence spectra of octapeptide aerosol particles using an UV-APS connected to a rotating drum. Octapeptides, organic molecules containing eight amino acids and present in cells, were used as a proxy to study the aging of tryptophan and results suggest bioaerosols exposure to typical ozone concentrations (~150ppb) decrease tryptophan fluorescence intensity and affects PBAP detection. Laboratory experiments cannot always reproduce the wide variety of environmental conditions and stressors that can affect the metabolism state of microbes, and hence their autofluorescence. Joly et al. (2015) studied the survival rate of multiple bacterial (e.g. *Pseudomona syringae*, *Sphingomonas sp. And Arthrobacter sp.*) and yeast (e.g. *Dioszegia hungarica*) strains isolated from cloud water upon exposure to oxidants (e.g. H_2O_2), solar light (e.g. UV radiation), osmotic shocks (e.g. multiple NaCl concentrations) and freeze-thaw cycles. Among these stressors, the freeze-thaw cycles affected most the survival rate (quantified as the quotient of the colony forming unit (CFU) counts before and after exposure to each stressor dose) of bacterial cells. *Arthrobacter sp.* showed the lowest survival rates (< 20%) per cycle, and the highest survival rate of all bacterial strains was observed at 10^8 cell mL^{-1} (highest concentration), suggesting that high cell concentrations lead to cell aggregation and provided protection against freeze-thaw cycles. The survival rate of the yeast *Dioszegia hungarica* was mostly affected by UV radiation showing the effect of each stressor in the survival rate of cells may depend on the characteristics of each cell. Even though the survival rate and the intrinsic fluorescence intensity of bioaerosols have not been correlated, multiple stressors can be affecting bioaerosols LIF detection and these issues regarding the use of LIF need to be resolved to fully understand their PBAP detection efficiency over the wide range of atmospheric conditions and PBAP population composition (Toprak and Schnaiter, 2013; Hernandez et al., 2016).

The aims of the study were to (i) develop an effective and reliable FCM detection and quantification protocol for bioaerosol; (ii) apply the protocol to understand ~~bioparticle~~bioaerosol populations and their variability ~~in the metro Atlanta area~~ during different meteorological conditions, and, (iii) compare FCM and WIBS-4A results to have a better understanding of PBAP day-to-day variability. To our knowledge, this study is the first to develop a FCM protocol to identify and quantify well-defined speciated bioaerosols populations from samples collected from a modified state-of-the-art biosampler. LIF sampling of bioaerosol side-by-side with established and quantitative biology tools (FCM and EPM) was conducted to assess the LIF detection capabilities toward different bioaerosol populations and under atmospherically-relevant conditions during this study. Atlanta is selected as a case study for PBAP sampling, as it provides a highly populated urban environment surrounded by vast vegetative areas; this and the broad range of temperature and humidity ensures a wide range of PBAP population composition, state and concentrations. All the samples collected are compared side-by-side to concurrent WIBS-4A data collected over the same time period.

Formatted: Font: 12 pt, Bold

2. Instrumentation and Methodology

2.1 Bioaerosol Sampler

Sampling was performed using the SpinCon II (InnovaPrep LLC, Inc.) portable wet-walled cyclone aerosol sampler. Aerosol is collected by inertial impaction with a recirculating liquid film in the cyclone; evaporative losses ~~of thr filmare~~are compensated so that the sample volume is maintained constant during a sample cycle. The particle collection efficiency for 1µm, 3µm, 3.5µm and 5.0µm particles is about 47.3±2.1%, 56.1±3.9%, 14.6 ± 0.6 and 13.8 ± 2.2%, respectively (Kesavan et al., 2015). However, the experiments conducted using 1µm PSL and 3µm PSL, 3.5µm oleic acid and 5.0µm oleic acid particles not necessarily quantify the collection efficiency of biological particles in this size range. Even with a lower efficiency than any impingement sampler, SpinCon has a better performance (product of the flow rate and the sampling efficiency) than any impingement sampler due to its high volumetric flow rate, which make it more suitable for bioaerosols detection (Kesavan et al., 2015). The efficiency, power consumption and performance of 29 biosamplers were analyzed by Kesavan et al. (2015) to determine which are best suited for indoor or outdoor sampling. The study concluded biosamplers effectiveness will be determined by their performance in the size range of interest, rather than just by looking its sampling efficiency. Furthermore, Santl-Temkiv et al. (2017) recently studied SpinCon retention efficiency towards sea water heterogenous and pure cultured *P.agglomerans* populations (~ 10^5 cells mL^{-1}) after 1 hr sampling period by comparing FCM-derived concentrations (using SYBR green stain) before and after the sampling period. SpinCon retains 20.6±5.8% of the *P.agglomerans* concentration, whereas 55.3±2.1% of the sea water microbial concentration is retained after sampling for ~~1hr.~~1h

In our study, the biosampler was run at 478L min^{-1} for 4hr sampling cycles. Phosphate-buffered saline (PBS) 1X pH 7.4 solution was used and the instrument compensated evaporation by supplying Milli-Q water to maintain the PBS concentration constant. Upon termination of each sampling cycle, the instrument was programmed to dispense the sample in a 15mL centrifuge tube. Then, 10µl of formalin (37 wt.% formaldehyde) per mL of solution was added to every sample for preservation and samples were stored at 4°C. Given the long sampling times and the low concentration of PBAP, the fluid supply system of the instrument was modified and a cleaning protocol (CP) has been developed, which is described below.

SpinCon II ~~H_2O~~water and PBS supply bags were replaced by two 2L autoclavable Nalgene bottles (Thermo Scientific Inc.) with antimicrobial tubing, connectors and a small HEPA filter connected to vent and prevent coarse and submicron particles contamination (Figure 1). Bottles were autoclaved and filled with Milli-Q water and PBS, beforehand sterilized with 0.2µm pore bottle top filters (Thermo Fisher Inc.)

and transferred inside a biosafety cabinet. An aliquot of each fluid obtained after preparation was evaluated for sterility by EPM and FCM.

The cleaning protocol (CP) of the biosampling system consists of two phases. During phase one, all acrylic windows and the outside of the collector/concentrator were cleaned with ethanol 70 wt. %. Then, the instrument inlet, outlet, and the inside of the collector/concentrator was cleaned with ethanol 70 wt. %. In the second phase, the SpinCon II inlet was connected to a HEPA filter to provide a particle-free source of air to the sampling system; the instrument was then washed with ethanol 70 wt.%, 10 wt.% bleach solution, PBS and Milli-Q H_2O, respectively. The wash consisted of a rinse, a 2 minutes sample and filling the instrument collector/concentrator with the fluid in use (i.e., bleach solution, ethanol, PBS and Milli-Q H_2O). The collector/concentrator was drained after 1 minute. The above were repeated for the remaining fluids, taking 5 minutes per fluid. Overall, the CP requires 45 minutes; upon completion, a blank is obtained to constrain the residual contamination levels after cleaning (described below). Finally, the HEPA filter was disconnected, instrument inlets and outlets were sealed and the inlet tube was cleaned with ethanol 70 wt.% to be ready for rooftop sampling. SpinCon II was rinsed with ethanol 70wt.% after each sampling episode and the cleaning protocol was applied before each sample.

Several blanks were obtained to quantify the levels of PBAP contamination in the fluids and sampler, and to ensure that they were sufficiently low to not bias the detection, identification and quantification of the PBAP. Furthermore, an instrument blank was obtained after a CP to constrain residual particles, by running the sampler for 2 minutes, while sampling air with a HEPA filter connected to the inlet of the SpinCon II. Another blank was collected to characterize any contamination of biological particles from the supply of PBS and water in the SpinCon II. This was done by operating the SpinCon II for a 4hr period with a HEPA filter connected to the inlet which completely cleans the air entering the wet cyclone from any bioparticles. All blanks were analyzed directly via FCM (Sect. 2.3) and EPM.

The volumetric flow rate within the SpinCon II was routinely calibrated by a VT100 Hotwire Thermo-anemometer (Cole Palmer Inc.) using a 3-hole round duct transverse approach. A 1 ¼" OD tube with the same diameter as the SpinCon II inlet was designed with 3 holes. Each hole was 60° apart from the other and the holes were perpendicular to the axial air flow direction of the tube. (Supplementary Information, Figure S1). Triplicates of flow rate measurements were taken in each hole at the center of the tube and averaged to determine SpinCon II volumetric flow rate (478.0 ± 6.4 L min^{-1}).

2.2 Flow Cytometry

During this study, a BD Accuri C6 flow cytometer (BD Bioscience Inc.) was used for Flow Cytometry. The instrument quantifies suspended cells in aqueous medium at three flow velocity modes (slow, medium and fast flow at 14, 35 and 66 µL min^{-1}, respectively). It excites particles with a 488nm laser and possesses

four fluorescence detectors: FL1 (533±30nm), FL2 (585±40nm), FL3 (> 670nm) and FL4 (675±25nm), which make it possible to analyze the fluorescence from multiple dyes concurrently. In this study, 2.5 µM SYTO-13 nucleic acid probe was added to the fixed samples and incubated for 15min in the dark at room temperature to stain biological particles. Additionally, 10µL of 15µm polystyrene bead suspension was added to the 1mL total volume samples as an internal standard for PBAP concentration and size quantification. The BD Accuri C6 was cleansed before each use with 0.2µm filtered Milli-Q water in fast mode for 10min; background particle counts were typically reduced to $1 \mu L^{-1}$. At the beginning of every experiment, a 1mL blank of the atmospheric sample without SYTO-13 and beads was analyzed, used in quantification calculations (Sect. 3.1). Each sample was run in slow mode for 5min. After each sample, the instrument was flushed with 0.2µm filtered Milli-Q water in slow flow for 1 minute (important for robust quantification of the typically low concentrations of the atmospheric samples). SYTO-13 fluorescence intensity was quantified by the FL1-A detector and used in combination with other parameters (FSC-A & SSC-A) to constrain the PBAP populations present. FSC-A measured forward (0° ± 13°) scattering and is used to characterize the size of particles; SSC-A measured the side (90° ± 13°) scattering and is used to characterize the internal complexity (non-sphericity/shape) of particles. A 80,000 unit intensity FSC-H threshold (default FSC-H threshold value suggested by the manufacturer to minimize the effect of noise) was set in the instrument during data acquisition to minimize the effects of noise on bioparticle counts. The FSC-H channel (where H denotes height), measures single-particle forward scattering (FSC) intensity based on the peak (maximum point) of the voltage pulse curve recorded when a single particle goes through the interrogation point in the flow cytometer, whereas FSC-A, where A denotes area, measures single-particle FSC intensity based on the area below the curve of the recorder pulse. When the 80,000 unit FSC-H threshold is defined, only signals with an intensity greater than or equal to threshold value will be processed, and this could affect the statistics and detection efficiency of the flow cytometer toward small particles (≤ 1µm). Experiments conducted with 1.0µm polystyrene beads suspension (Supplemental information; Figure S16) have shown that 1.0µm beads have FSC-H intensities above the 80k threshold, no particle losses is observed, and beads estimated concentration agree with the reported by the manufacturer (~6×10^7 mL^{-1}; Life Technologies, Inc.) The FCM data from each sample was analyzed using the Flow Jo software (https://www.flowjo.com/solutions/flowjo) to gate and quantify bioparticles population. The same procedure was used to analyze the PBS, Milli-Q water and blanks.

2.3 LIF detection of PBAP

The WIBS-4A (referred to henceforth as "WIBS") is a single biological particle real time sensor, which measures particle light scattering and autofluorescence in an approximately 0.5 – 15µm particle range (www.dropletmeasurement.com). Particles are initially sized using the 90-degree side-scattering signal

from a 635 nm continuous-wave diode laser. The scattering intensity is directly related to particle diameter and was calibrated prior to deployment using polystyrene latex sphere calibration standards (PSL with 0.8, 0.9, 1.0, 1.3, 2.0, 3.0 µm diameter, Thermo Scientific Inc.). The WIBS optical size therefore refers to PSL material with a real refractive index of 1.59. Healy et al. (2012) determined WIBS-4 counting efficiency by aerosolizing standardized concentrations of PSL sphere of specific sizes (e.g. 0.3, 0.4, 0.56, 0.7, 0.9 and 1.3µm) and compared WIBS-4 total counts against PSL counts detected by the condensation particle counter (CPC). Results show WIBS-4 possesses a 50% counting efficiency for 0.5µm particles and detects 100% of the PSL particles above 0.7µm when it is compared to the CPC counts. The 280nm and 370nm pulsed Xenon flashtube UV lights in the WIBS cause the particles to autofluoresce (i.e., excite the chromophores preexisting in the PBAP and do not rely on a fluorescent dye as done in FCM). Then, fluorescent emissions are measured at three wavelength channels, which following the nomenclature of Perring et al. (2015) are: (*i*) channel A ("FL1_280" in previous studies; Robinson et al., 2013), which refers to the detected emission between 310-400nm after excitation at 280nm, (*ii*) channel B ("FL2_280" in previous studies), which refers to the detected emission between 420-650nm after excitation at 280nm, and, (*iii*) channel C ("FL2_370" in previous studies), which refers to the detected emission between 420-650nm after excitation at 370nm. The resulting autofluorescence from 280nm excitation is affected by the presence of tryptophan, tyrosine and phenylalanine ~~aminoacids~~amino acids in the PBAP (Pöhlker et al., 2012). Similarly, the resulting autofluorescence from the 370nm excitation is influenced by the presence of riboflavin and co-enzyme Nicotinamide Adenine Dinucleotide Phosphate (NAD(P)H) within the cells.

Biological and non-biological particles can be discriminated by using a fluorescent intensity threshold; here the threshold is determined with the Gabey et al. (2010) method and with modifications by Perring et al. (2015) as follows. Particles with fluorescence intensities below the fluorescence threshold in all channels are categorized as non-fluorescent (NON-FBAP). Particles that fluoresce above the threshold in only one channel are named with a single letter (e.g. A, B or C); particles that fluoresce in two channels are named with the two channel letters (e.g. AB, AC or BC), while particles that fluoresce in all channels are categorized as type ABC. Furthermore, the total FBAP concentration is defined as the sum of the concentration in the seven FBAP categories defined above. This approach was applied by Hernandez et al., (2016) to pure culture PBAP (bacteria, fungal spores, pollen) to study their correspondence to FBAP types; bacteria tend to be detected by type A, and fungal spores and pollen by type AB and ABC. However, bioaerosol classification is instrument-specific and particle size dependent (Hernandez et al., 2016; Savage et al., 2017).

~~Several studies have used the Perring et al. (2015) FBAP categories to characterize PBAP in multiple environments across the globe (Yue et al., 2017; Gosselin et al. 2016 ;~~ Multiple environments have been

studied using the Perring et al. 2015 FBAP types, including rural, urban and highly vegetated locations. In the Southeastern US, the total FBAP concentration~~Yu et al., 2016). Perring et al. (2015), using a WIBS 4, studied atmospheric PBAP onboard a Skyship 600 aircraft operating between 300m and 1km above ground level at 10 geographic regions across the United States; the study concluded that type AB (~30%) and ABC (~25%) is the most abundant of FBAP particles in the Southeastern US (East Texas to Central Florida), and AB (~1.9 µm) and ABC (~2.6 µm) median sizes are characteristic of mold spores (fungal spores of unknown amount of species predominant on humid and warm environments; www.cdc.gov). In addition, FBAP concentrations in the Southeastern US~~ range from 2×10^4 to 8×10^4 m^{-3}, constituting 3-24% of the total supermicron particle number between 1 and 10µm diameter. ~~In the Southwestern US, Perring et al. (2015) shows AB and ABC types contribute less due to a higher relative contribution by types B (~25%), BC (~20%) and C (~5%), and total FBAP constitute 5-10% of the total supermicron particles. Furthermore, Perring et al. (2015) found the concentration of ABC type PBAP on the surface and aloft did not vary throughout the Southeastern US. In the highly vegetated Rocky Mountains Gosselin et al. (2016) found (using a WIBS 3) that ABC type particles always are a significant fraction of FBAP (at least 20%) and are especially~~In the highly vegetated Rocky Mountains, ABC type particles are enhanced during rainy days (during or post-rain events) to ~ 65% of the total FBAP, owing to the release of wet-ejected fungal spores following precipitation (Gosselin et al., 2016). On the contrary, in the highly populated city of Nanjing, China all FBAP types, except type C, correlated with black carbon concentrations, suggesting a strong interference by combustion sources (Yu et al., 2016). ~~Huffman et al., 2013). However, during dry days, types BC and C increase their relative fraction to ~30% and ~40%, respectively (Perring et al., 2015). Limited studies have looked closely at the FBAP categories in urban environments. In Naijing, China, Yu et al. (2016) observed that types B (~45%), BC (~25%) and C (~15%) dominate the FBAP concentrations during autumn. All FBAP types, except type C, correlated with black carbon and $PM_{0.8}$ concentrations (particle mass with diameter below 0.8µm), suggesting a strong interference by combustion sources; Type C PBAP ($6.6\times10^5 \pm 5.5\times10^5$ m^{-3}) was considered more representative of bioaerosols, although with unknown interference from abiotic particles. Similarly, Yue et al. (2017) found a dominance of type B PBAP (~66% of total FBAP) during clean and polluted events in wintertime Beijing, China; interestingly, the FBAP contribution to the total particle concentration is higher during polluted events (13-24%) than during clean events (12-14%). FL1 type particles (sum of types AC, ABC, AB and A) are more abundant in clean periods (~25%) than in polluted periods (10.1%), while the fraction of type C FBAP is higher during polluted periods (~20%) than during clean periods (~5%).~~ A detailed explanation of the above-mentioned studies using Perring et al. 2015 approach is also included in the section SI.20 of the supplemental information.

2.4 Location of sampling site and sampling frequency

Formatted: Font color: Auto

Formatted: Font color: Auto

Bioaerosol sampling was conducted between April 7 and May 15, 2015 at the rooftop sampling platform of the Ford Environmental Sciences and Technology (ES&T) building at the Georgia Institute of Technology campus in Atlanta, GA. The site, which was located at the heart of a major urban environment, is surrounded by dense forested areas in the southeastern USA: the Oconee National Forest (South East), the Chattahoochee National Forest (North), and the Talladega National Forest (West). The WIBS was operating continuously throughout the same period, sampling bioaerosol from a 15 ft. long and ¼ in. ID conductive tubing inlet fixed 8 ft. above the sampling platform floor. The SpinCon II was placed in the platform during sampling episodes with its inlet facing South. Three 4-hour samples per week were collected with the Spincon II sampler over the 5-week period (4 h sampling between 10am and 5pm; Table 1). Meteorological data acquired from the same platform provided wind speed, wind direction, relative humidity (RH), temperature, total hourly rain and UV radiation index with a 1min resolution.

Formatted: Font: 12 pt, Bold

3. Data processing and Analysis

3.1 FCM data processing

All blanks collected showed contamination levels that did not exceed 1% of the PBAP quantified in the subsequent atmospheric samples. The 2-minute instrument blanks obtained after the CP and the HEPA filter washes was $1.06\times10^{3} \pm 7.37\times10^{2}$ mL^{-1} and $9.22\times10^{2} \pm 1.24\times10^{2}$ mL^{-1}, respectively, which are negligible accumulations compared to the $2.55\times10^{5} \pm 1.14\times10^{5}$ mL^{-1} average PBAP concentration quantified in the atmospheric samples. The concentration of PBAP in the blanks was also confirmed with microscopy (not shown). Based on this, we are confident that the CP protocol and procedure to replace the working fluids ensured sterility of the biosampler before each sampling.

FCM analysis of the samples was carried out as follows. We obtain the fluorescence intensity (from each of the 4 fluorescence detectors), forward scattering and side scattering intensity for all the particles suspended in the samples. A gating procedure was used to determine the fluorescence levels associated with detecting only particles containing SYTO-13 (hence, a PBAP) and background fluorescence from non-stained particles. The procedure (Supplemental information, SI.2 and SI.3) consists of 3 steps: (a) fluorescence threshold determination, (b) population gating, and, (c) biological/non-biological particle discrimination in the population(s) within the threshold (e.g. LNA PBAP, Section 4.1). The fluorescence threshold was determined using an atmospheric sample without SYTO-13 collected before each FCM analysis, as a blank. Based on the fluorescence responses obtained, we determine the FL1-A fluorescence intensity value for which 99.5% or 99.9% of the (unstained) particles of the blank autofluoresce below the chosen value. This FL1-A intensity, called “fluorescence threshold”, was determined for each sample (supplementary information, Figure S2a and S2b). The determination of the fluorescence threshold

involved selecting the most conservative value that maximizes inclusion of biological particles and minimizes the inclusion of non-biological particles, including those that may be subject to background fluorescence or unspecific binding of SYTO-13 (Diaz et al., ~~2009~~2010; Müller et al., 2010). We found out that threshold values for the 99.9% approach were substantially higher than 99.5% approach in multiple sampling events and comparable to the fluorescence intensities observed for stained pure cultures (~10^5 units), which means that the 99.9% threshold values will miscount pure cultures as non-biological. Consequently, we set the fluorescence threshold to the highest fluorescence intensity value observed by the 99.5% approach (41,839 units; supplementary information, Figure S2b), applied it to all collected samples; henceforth named the 42k FL1-A threshold. The 42k threshold value aims to minimize any abiotic interference as it maximizes biological particles quantification. A fixed value has been chosen and applied to all samples given that having a different threshold value for each sampling event may result in quantification biases as bioaerosols with strong autofluorescence (e.g. pollen, fungal spores) can increase the threshold value and affect PBAP quantification in the population(s) within the threshold. The BD Accuri C6 flow cytometer used for the analysis of the samples maintains constant pre-optimized photomultiplier voltages and amplifier gain settings. As a result, the fluorescence intensity of particles is consistent from day-to-day, and the fluorescence intensity of a specific biological particle population having the same metabolic state and physiological characteristics must not show day-to-day variability (www.bdbiosciences.com). Under the 42k threshold approach PBAP concentrations in the population(s) within the threshold (e.g. LNA, Section 4.1) can be overestimated by up to a 0.5%. Furthermore, FCM experiments conducted with unprocessed Arizona Test Dust (ATD) show that the FL1_A intensity distribution of SYTO-13 stained ATD particles is very similar to unstained ATD particles, and 100% of the SYTO-13 stained ATD particles stay below the 42k threshold (supplemental information, Figure S14a and S14b), supporting the 42k threshold effectiveness to filter out abiotic particles.

Once the FL1-A threshold was determined, plots of FL1-A vs. SSC-A and FL1-A vs. FSC-A are used to define clusters of bioparticles with fluorescence that exceed the FL1-A threshold and a characteristic optical size (obtained from the FSC-A intensity) or particle shape/complexity (obtained from the SSC-A intensity). FL1-A vs. SSC-A plots were used to define the populations of bioparticles for PBAP quantification as clusters using SSC-A parameter were more defined and showed better spatial resolution than using FSC-A parameter. The limits of each population were also determined with Flow Jo (www.flowjo.com), using 2% contour plots (supplemental information; Figure S3) generated by equal probability contouring (i.e., 50 contour levels so that the same number of cells fall between each pair of contour lines). Populations above the FL1-A threshold value (41,839 FL1-A units) were considered biological (Section 4.1; e.g. HNA); the particles in the population within the threshold value (Section 4.1; e.g. LNA) having a FL1-A intensity greater than 41,839 units were counted as biological to determine the

PBAP counts in the population. The total PBAP counts were considered as all particles counts having FL1-A fluorescence intensity above the determined threshold value minus the 15µm beads internal standard having FL1-A fluorescence intensity above the determined threshold value. The 15µm beads of known concentration and particle size allows for calibrating the optical size (supporting information, SI.7) of the bioparticles, as well as their concentration and departure from sphericity. The 15µm beads population showed fluorescence intensities comparable to the determined fluorescence threshold after been stained with SYTO-13 as it is known that molecular stains can be adsorbed on the surface of polystyrene beads (Eckenrode et al., 2005; Rödiger et al., 2011). The relatively high fluorescence intensity of the 15µm beads show populations within the threshold value (e.g. LNA, Section 4.1) cannot be rule out as being affected by unspecific staining of abiotic particles. However, populations above the threshold value (e.g. HNA, Section 4.1) should not be affected by such abiotic interferences.

Formatted: Font color: Text 1

3.2 WIBS data processing

15-minute average total aerosol and FBAP size distributions were obtained from the WIBS. FBAP was distinguished from the total aerosol using the Gabey et al. (2010) "trigger threshold" approach, which is applied as follows. First, the average "electronic fluorescence noise" and its standard deviation is determined for each channel (A, B, C) performing the Force Trigger (FT) calibration which consist to operate the WIBS without flowing air through the system. The FT calibration, carried out every 24hr, is critical for determining the lowest particle autofluorescence levels that robustly exceeds instrument electronic noise. FT calibrations measured the particle-free air background autofluorescence in the three WIBS channels (e.g. A, B, C), and measurements recorded the fluorescence intensity for 500 excitation flash events (Ziemba et al., 2016; Tropak and Schnaiter, 2013; Gabey et al., 2010). The threshold for each detector is then equal to the average fluorescence plus 2.5 times its standard deviation; particles with fluorescence intensities above this threshold value are classified as FBAP. Then, Perring et al. (2015) approach (Section 2.3) is applied to determine the combination of thresholds that provide the maximum concentration of PBAP and minimal interference from abiotic particles, which still remains an area of active research. ~~WIBS-3 and WIBS-4 models have been actively studied to determine which channel best detect bioaerosols and to cluster different types of PBAP (Robinson et al., 2013; Crawford et al., 2014; Gabey et al., 2010). Both models use filtered xenon flash lamps to excite particles at 280nm and 370nm wavelengths and detect PBAP autofluorescence in two regimes (For WIBS-3, FL1: 320-600nm and FL2: 410-600nm; For WIBS4, FL1: 310-400nm and FL2; 420-650nm). Three separate fluorescence channels for each model: (i) channel A: detection in FL1 following 280nm excitation, (ii) channel B: detection in FL2 following 280nm excitation and (iii) channel C: detection in FL2 following 370 nm excitation, are then available for FBAP determination. The main difference between WIBS models is that the fluorescence detection regimes overlap in channels A and B for the WIBS-3, but not for the WIBS-4. WIBS-3 FBAP quantification cannot~~

~~be compared directly with WIBS-4 due to channel A and B overlap, but FBAP detection in all channels have been consistent between both models (Robinson et al., 2013). WIBS-4 contains two switchable gain settings (e.g. high gain (HG), low gain (LG)), allowing it to measure 0.5μm to 12μm particles in HG and 3μm to 31μm particles in LG setting. On the other hand, the second generation of the WIBS-4, named WIBS-4A, maintains single gain settings and evaluates particles between 0.5μm and 20μm (Fennelly et al., 2017~~It is important to note that the Gabey et al. (2010) threshold approach and the Perring et al. (2015) FBAP types were applied to the WIBS-4A data and should not be directly compared to FBAP quantifications performed by the WIBS-3 in previous studies, owing to the channel A and B overlap on the latter. A detailed comparison between WIBS-3 and WIBS-4 models, as well as PBAP detection by both models, is further discussed in the supplemental information (SI.20).

~~Gabey et al. (2011) concluded, using a WIBS-3, that channel C was most efficient in quantifying FBAP either in the Borneo tropical forest or in the urban environment of Manchester, UK. Healy et al. (2014) found higher channel A FBAP concentration in Killarney, Ireland using WIBS-4. Pure culture experiments with WIBS-4 have shown high detection efficiency of channel A toward *Pseudomona syringae* bacteria (Tropak et al., 2013). Hernandez et al. (2016) used WIBS-4 to test the intrinsic fluorescence fingerprints of 29 fungi, 13 pollen and 15 bacteria species and suggested channel A is most suitable for discriminating bacteria and fungi, channel C is most suitable for pollen and channel B can be influenced by abiotic particles. In addition, among FBAP categories (Perring et al., 2015) bacteria is mainly detected as type A, fungal spores shown multiple fluorescence types (e.g. A, AB, BC and ABC) and pollen is mainly detected as type BC and ABC. However, PBAP detection effectiveness by specific channels varies considerably between instruments, which suggests a thorough calibration may be necessary. Furthermore, Savage et al. (2017) used WIBS-4A to show FBAP fluorescence also varies with particle size, especially for pollen and fungal spores and proposed pathways of change by which particles may transition from type A or type B to type ABC as they increase size. FBAP type variation with particle size is important to consider as the approach of Perring et al. (2015) is used to better understand what FBAP type is best detected (e.g. bacteria, fungal spores, pollen).~~

In this study, thresholds for each channel were determined daily, and the total particle concentration, FBAP types (e.g. A, B, C, AB, BC, AC, ABC) concentrations and the total FBAP concentration (sum of the seven FBAP types) were used. From the data, 4h-averaged size distributions (using 15-minute average data) were generated for the total particles and all FBAP types in the 1-10μm range during the time SpinCon II run. Subsequently, WIBS overall sampling efficiency (aspiration efficiency + transport efficiency) was calculated using the Particle Losses Calculator (Von der Weiden et al., 2009) and applied to the 1-10μm size distributions for the sampling characteristics in our setup (15ft. sampling line with ¼ in. ID and 2.3 L min^{-1} flow rate; Figure S4a**)**. The sampling efficiency was calculated to be 67% for 5μm particles, with

larger losses as size increased to 10µm. (supplemental information, FigureS4b). FCM and WIBS total particles and PBAP comparison was constrained to the 1 to 5µm range being the size overlap of both techniques. Also, the fractional composition of FBAP (based on number concentrations) was calculated to characterize its daily variability (Section 4.2), and compared against the daily variability of PBAP from the FCM analysis (Section 4.4).

4. Results and Discussion

4.1 FCM biopopulation identification and quantification

When the FCM results are plotted in terms of FL1-A intensity versus SSC-A intensity, four populations (Figure 2) emerge above the threshold gating process: low nucleic acid (LNA) particles, high nucleic acid (HNA) particles, pollen and the 15µm internal standard beads. EPM and SEM pictures (Supplementary Figures S5, S6, and S7) confirm the presence of these heterogeneous populations. Previously, LNA and HNA populations were identified in FCM of aquatic samples with the use of the SYTO-13, SYBR green and DAPI nucleic acid stains (Wang ~~Y.~~ et al., 2010; Bouvier~~, T.~~ et al., 2007; Lebaron~~, P.~~ et al., 2001); corresponding populations in atmospheric PBAP have not been identified before. Below we focus on each population to further ~~identify them as pollen, fungal spores, bacteria and other fragments.~~understand the identified populations of biological particles.

The HNA size distributions are dominated by 3-5µm particles (mean diameter: 4.15 ± 0.06 µm; Supplemental Information, Figure S10) and the total concentration ~~strongly~~moderately correlated with RH. HNA were virtually non-existent during several extended dry periods (days with average RH < 70% during sampling, e.g. 4/9, 4/22 and 5/15) and well defined during periods of high humidity, especially after rain events (days with average RH > 70% and T > 18 °C during sampling episode; e.g. 4/7, 4/14, 4/15). Both of these characteristics suggest that HNA particles correspond to wet-ejected fungal spores (e.g., from the Ascospores and Basidiospores genus; Oliveira et al., ~~2000~~2009; Li and Kendrick, 1995). The LNA size distributions are dominated by 2-4 µm particles (mean diameter: 2.99 ± 0.06µm; Supplemental Information, Table S1) and dominated Atlanta PBAP composition during dry days. ~~The LNA population shows SYTO-13 fluorescence intensities that are about one order of magnitude lower than the HNA population. The observed particle sizes are within the size range of airborne bacteria (Després et al., 2012) and the~~Many individual bacteria are likely in around 1µm, but the observed LNA particles are within the median aerodynamic diameter of culturable bacteria (~ 4µm) in continental sites (Despres et al., 2012). Bacteria in the atmosphere can be co-emitted together with larger particles (e.g. soil, plant fragments) and occasionally they are observed as clumps of bacteria cells (Burrows et al., 2009). In addition, several bacterial species observed in the atmosphere (Delort and Amato, 2018; Monier and Lindow, 2003; Baillie and Read, 2001) are within this sizes range (e.g., *Sphingomonas spp.*: 1.0 - 2.7µm; *Methylobacterium spp.*: 1- 8 µm,

Formatted: Font: Italic

Pseudomona syringae: ~2.5µm, and *Bacillus anthracis*: 3-10µm), supporting LNA population may represent single or agglomerated bacterial cells. However, it is clear that heterogeneous populations will probably contain multiple types of microorganisms and that may be the case in the LNA population. The LNA population also shows SYTO-13 fluorescence intensities that are about one order of magnitude lower than the HNA population.

Formatted: Font: Italic

It is known that pollen may burst into tiny fragments when is suspended in water (e.g., Augustin et al., 2012; Taylor et al., 2007~~). Therefore, pollen may fragment during sampling and processing of samples in the FCM, increasing the concentration of LNA particles and biasing concentrations.~~), potentially increasing the concentration of LNA particles and biasing concentrations. Although 0.2µm – 5µm pollen fragments can be generated upon rupture, pollen (e.g. Birch, Ryegrass, Oak, Olive) mainly breaks apart into submicron fragments by hydrolysis and favors fragmentation into small submicron (<1µm) particles (Taylor et al., 2007; Bacsi et al., 2006; Grote et al., 2003), not considered in our FCM analysis. An additional factor to consider in pollen fragmentation is the number of fragments generated per pollen grain. FCM applied to ragweed pollen suggests a 1:2 pollen-to-pollen fragments concentration ratio (Supplementary information, Table S2). Also, calculations based upon FCM-derived ragweed pollen and pollen fragments concentrations during this study (considering the total pollen mass added to the sample, 15µm mean diameter previously determined by Lin et al. (2013) and unit density) suggest approximately 67% of the ragweed pollen grains were intact after hydration and that each fragmented grain generates ~5 pollen fragments; in agreement with Bacsi et al. (2006), 35% of ragweed pollen fragments upon hydration. Overall, ragweed pollen results suggest FCM experiments do not have a considerable impact in pollen fragmentation and that pollen fragmentation will have a negligible effect on LNA concentrations. Ragweed pollen is one of the most abundant wind-driven pollen species in the United States and its emission peaks during fall, but can be also present during late spring and summer. It is representative of the pollen species we see in the Atlanta area (Darrow et al., 2012) and results suggest pollen fragmentation would not generate a substantial amount of fragments. The low collection efficiency of SpinCon toward large particles (<14% for diameters above 5µm) and that pollen concentrations in our samples are generally two orders of magnitude lower than LNA concentrations (Figure S22; supplemental information) suggest a negligible effect of pollen fragments in LNA biological particle quantification. Pollen concentrations are 100-1000 times lower than bacteria concentrations in the atmosphere (Hoose et al.,2010). At least 100 supermicron (>1µm) pollen fragments will have to be released per pollen grain to considerably influence the LNA population, which has not been observed. Also, EPM results showed intact pollen and limited amounts of small debris among the particles identified in the atmospheric samples collected for this study. Particles with fluorescence intensities above the FL1-A threshold value in the LNA population were counted as biological, giving us the PBAP counts

Formatted: Font: Italic

Formatted: Font: Italic

within the LNA population and will be referred henceforth as the "~~bioLNA~~LNA-AT" population (Figure 2~~).~~), where "AT" refers to above threshold.

A population of strongly fluorescing and very large particles (10-20µm, avg. average geometric mean diameter 12.3 ± 1.7µm) was identified (Figure 2). This population also strongly autofluoresces in the FCM when SYTO-13 was not added to the sample (SI.7, Figure S11). All together this indicates a population of pollen particles, as they are known to contain cell wall compounds (i.e., phenolic compounds, carotenoid pigments, Phenylcoumarin) that fluoresce more strongly than the proteins and cytosolic compounds responsible for bacteria/fungi autofluorescence (Pöhlker et al., 2012; Hill et al., 2009; Pöhlker et al., 2013). The pollen population was not well-defined during all sampling events; whenever present, pollen was characterized by concentrations (~10^2 m^{-3}) consistent with reported values (Despres et al., 2012), which are also much lower than ~~bioLNA~~LNA-AT and HNA concentrations. As a result, pollen population was systematically gated using a perfect square between 10^6 and 10^8 intensity units in the FL1-A vs. SSC-A plot for each atmospheric sample. ~~bioLNA~~LNA-AT, HNA and pollen counts, acquired by the 42k threshold approach were used to calculate liquid-based (mL^{-1} of sample solution) and air-based (m^{-3} of air) concentrations for each bioaerosol population as detailed in the Supplemental Information**.** The total PBAP concentration on each sample consisted of all non-bead particles above the 42k fluorescence threshold given that a non-negligible biological particle concentration was not constrained in the gated populations. Even though the 2% contour plots effectively allowed population gating, 16.5 ± 7.3% of the total PBAP are not attributed the identified populations. The biological particles not constrained by FlowJo 2% gating, henceforth named as the "unclassified" bioparticles, showed the highest concentrations when both HNA and LNA populations are densely populated (4/16, 4/28 and 5/14; Figure 5). The lowest concentrations were observed when just the LNA population is identified (4/9, 4/22, 5/15; Figure 5) and when the LNA and HNA populations are identified after the rain event on 4/14. The observed behavior shows that the unclassified bioparticle concentrations is linked to the heterogeneity of the biological populations and the concentration of the gated populations (e.g. HNA, LNA and Pollen). The "unclassified" bioparticles concentration ranges from 8.1 x 10^2 m^{-3} to 1.3 x 10^4 m^{-3} (avg. 4.2 x 10^3 ± 3.3 x 10^3) and they are not constrained to a specific size range. Most of the unclassified bioparticles are far from the centroids of the gated populations. They can indeed be formed by fragmentation or accretion, or also be related to plant debris (i.e., irregular bioparticles) that are characterized by a very broad size, internal complexity and nucleic acid content distributions. In addition, we must note that additional concentration corrections are required owing to the sampling efficiency of the SpinCon II, but will be considered in sections 4.3 and 4.4.

Formatted: Font: Italic

Before SpinCon II sampling efficiency corrections are applied, FCM total particle concentrations range from 2.6×10^4 m^{-3} to 2.9×10^5 m^{-3}, with increasing concentrations toward the end of the sampling period. In addition, total PBAP concentration averaged $2.4 \times 10^4 \pm 1.1 \times 10^4$ m^{-3} (coefficient of variation, CV, 13%; defined as the standard deviation over a triplicate FCM measurements over the average concentration). ~~BioLNA~~LNA-AT ranged between 6.8×10^2 and 2.9×10^4 m^{-3} (average: 1.1×10^4 m^{-3}; CV: 20%), HNA(fungal spores) between 4.7×10^3 and 1.9×10^4 m^{-3} (average: 1.1×10^4 m^{-3} ; CV: 15%) when above the detection limit (n=12), and pollen from 1.3×10^2 to 1.2×10^3 m^{-3} (average: 3.6×10^2 m^{-3}; CV: 21%). These concentration levels are consistent with microscopy-based studies in urban environments for bacteria (e.g., $1.7\times10^4 \pm 1.3\times10^4$ m^{-3} in springtime Birmingham, UK; (Harrison et al., 2005); fungal spores ($1.8\times10^4 \pm 1.1\times10^4$ m^{-3} in Vienna, Austria between April-June; Bauer et al., 2008); and pollen (between 5.69×10^2 m^{-3} to 6.144×10^3 m^{-3} in Medellin, Colombia; Guarín et al., 2015). Also, additional experiments performed in September 2015, described in Figure S7 of the supplemental information (supplemental information, SI.6), showed that EPM and FCM-based quantifications agree within an order of magnitude. This is consistent with Lange et al. (1997), whom also found that FCM gives higher quantifications than EPM microscopy when studying *P. aeruginosa* pure cultures and airborne bacteria collected from a swine confinement building in Iowa, USA.

To better understand SYTO-13 fluorescence intensity differences between the identified (e.g. ~~bioLNA~~LNA-AT, HNA and pollen) populations in the atmospheric samples and their metabolic/stress state, FCM experiments were conducted with air-isolated bacteria (F8 strain; De Leon Rodriguez, 2015), ragweed pollen and yeast (*S. cerevisiae*; Y55 strain) mixtures to compare the SYTO-13 fluorescence intensity and the scattering properties of the pure cultures to those seen in the atmospheric samples. Pure cultures and atmospheric samples are summarized in Tables S3, S4 (supplementary information; FCM pure culture experiments) respectively. The ~~bioLNA~~LNA-AT population showed SYTO-13 fluorescence intensity up two orders of magnitude lower than F8 bacteria. HNA (fungal spores) population showed an order of magnitude lower SYTO-13 fluorescence intensity than Y55 HNA yeast, and, within the same magnitude for the LNA Y55 yeast. The HNA and LNA yeast populations in the pure culture experiments (Figure S13a) have one order of magnitude difference in FL1-A fluorescence intensity and may represent yeast populations with different metabolic states. Atmospheric and ~~Ragweed~~ragweed pollen populations had similar SYTO-13 fluorescence intensities and Figure S13c shows pollen fluorescence intensity may go up to 10^8. The lower SYTO-13 fluorescence intensity of the atmospheric populations may be related to genetic material degradation from exposure to atmospheric stressors; depending on the physiological characteristics of each population (Zhen et al., 2013; Amato et al., 2015). Our results also agree with Guindulian et al. (1997), showing that *E.coli* overnight cultures have higher SYTO-13 fluorescence

intensity than starved *E.coli* population. Overall, FCM pure culture results suggest microbes starve in the atmosphere, leading to a possible reduction or leakage of the amount genetic material enclosed within each cell. Sampling can also stress cells, even disrupt the wall/membrane of the cell and lead to genetic material leakage (Zhen et al., 2013).

Pollen, HNA ~~(fungal spores)~~ and ~~bioLNA~~LNA-AT atmospheric populations showed different SYTO-13 fluorescence intensities. Pollen showed the highest fluorescence intensity**,** followed by the HNA and ~~bioLNA~~LNA-AT (fraction of LNA above threshold; Figure 2) populations, respectively (Figure 2; Table S4). Guindulian et al. (1997) FCM results with starved bacterioplankton from seawater samples treated with ~~DNAse~~DNase/RNase showed SYTO-13 fluorescence intensity can be related to the DNA content of starved bacterioplankton due to the low amount of RNA enclosed in starved cells. Taking in consideration our results and previous studies, we can suggest that Pollen, ~~bioLNA~~LNA-AT and HNA populations in the atmospheric samples are differenced by their DNA content, which can in part explain SYTO-13 fluorescence intensity difference between them. We also acknowledge DNA sequestration by bacteria, fungal spores and pollen may differ and their cell membrane characteristics will ultimately determine how much stress the cells will sustain before they completely rupture. SYTO-13 is a highly permeable stain and effectively detects nucleic acids (DNA and RNA) of bacteria endospores and vegetative cells (Comas Riu et al.,2002). Fungal spores have also been effectively stained by DNA/RNA probes (Bochdansky et al., 2017; Chen and Li et al., 2005), but some fungal spores might not be equally stained due to their harder cell wall, and chromatin-binding of DNA (Standaert-Vitse et al., 2015). Future work is needs to further study this.

4.2 WIBS total concentration and FBAP daily variability

WIBS-4A collected data continuously throughout the period; for comparison against the SpinCon II 4h liquid batch samples, WIBS data was averaged to the SpinCon II sampling times (Table 1). WIBS total particle concentration (1-5µm diameter) ranged from 2.0×10^5 to 1.0×10^6 m^{-3} in agreement with observed particle concentrations in previously studied urban environments during Spring/Summer months like Helsinki, Finland (UV-APS avg. 1.6×10^5 m^{-3}; Saari et al., ~~2015~~2014) and Karlsruhe, Germany (WIBS-4 avg. 6.9×10^5 m^{-3}; Tropak and Schnaiter et al., 2013). 4h average total particles concentrations in Figure 3a show particle concentrations declined during rain episodes (during or post-rain: e.g. 4/15, 4/16, 4/28, 4/29, 4/30) as wet removal of PBAP is most efficient. However, during dry (no rain) episodes total particle concentrations built up in the atmosphere. To better understand the day-to-day variability of different FBAP types, the seven Perring et al. (2015) FBAP categories (e.g. Type A, B, C, AB, AC, BC and ABC) were

667 studied plus the NON-FBAP type constituting particles that do not fluoresce in any channel (e.g. channel
668 A, B, C). NON-FBAP concentrations are one order of magnitude higher than FBAP concentrations, and
669 NON-FBAP, hence traced WIBS total particles throughout all sampling events (Figure 3a). Total FBAP
670 concentrations also show similar behavior to the total particle concentration (Figure 3a) and it suggests non-
671 biological particles can be biasing the total FBAP concentration. The variability of the total FBAP
672 concentration is mainly linked to type A and type B concentrations as overall they constitute the two largest
673 fractions to the total FBAP concentration (Figure 3b), and both FBAP types have previously misidentified
674 non-biological particles as FBAP (Tropak and Schnaiter et al., 2013; Yu et al., 2016). As a result, our study
675 considers the total FBAP concentration as the upper limit, and ABC type concentration as the lower limit
676 of FBAP concentration in Metro, Atlanta. Type B dominates the FBAP fractional composition (Figure 3b),
677 which has been linked to possible non-biological interferences from black carbon (Yu et al., 2016) and
678 polycyclic aromatic hydrocarbons (PAHs) emitted from combustion sources. Total FBAP fraction ranges
679 from 16% and 43%, and ABC fraction ranges from 1.3% and 9.2% of the total particles in the 1 to 5µm
680 size range. ABC type fractions and ABC type concentrations are within the values observed by Tropak and
681 Schnaiter (2013) using WIBS-4 in Karlsruhe, Germany; averaging 2.9×10^4 m^{-3} (when considering the sum
682 of AC and ABC types) and constituting 7% of total coarse mode particles (0.8µm-16µm).

683 ABC type concentrations show an interesting variability throughout the 15 sampling events, as
684 ABC reaches its maximum concentration on 4/14, on a warm and humid day after a rain event, concurrently
685 when the FCM HNA population also reaches its highest concentration – strongly suggesting ABC particles
686 are fungal spores. (Figure 3a, Table 1). Recently, Gosselin et al. (2016) used WIBS-3 in the Rocky
687 Mountains, Colorado showing ABC type fractional composition enhances after rain events to dominate the
688 total FBAP composition and the enhancement is correlated to mannitol and arabitol concentrations (fungal
689 spore tracers), which have been previously linked to Ascomycota and Basidiomycota spores emitted by the
690 wet-ejection mechanism (Elbert et al., 2007). In addition, ABC type constitute a considerable fraction
691 (~20%) of total FBAP during dry days in the Rocky Mountains possible because such highly vegetative
692 environments maintain a high background of fungal spores (Huffman et al., 2013). However, urban
693 environments like Metro Atlanta are not necessary dominated by fungal spores and its FBAP composition
694 will be affected by the biological sources close to city (e.g. forests), local emissions and meteorology. The
695 overall FBAP composition in metro Atlanta (Figure 3b) is dominated by type B (avg. fraction: 33 ± 9%),
696 type A (avg. fraction: 22 ± 5%) and type AB (avg. fraction: 22 ± 5%) particles. Type ABC constitute 12 ±
697 6% of the total FBAP and it reaches 30% on 4/14, comparable to values observed by Gosselin et al., 2016
698 in the Rocky Mountains. The dominance of type B particles has been observed in the polluted atmosphere
699 of Nanjing, China using WIBS-4A were type B constituted ~ 45% of the total PBAP and type B (~ 2×10^6

m^{-3}) concentrations were up to two orders of magnitude higher than type A concentrations (~5×10^4 m^{-3}) suggesting a high likelihood of interference from abiotic particle sources. However, Metro-Atlanta shows much lower total particle concentrations than Nanjing, China (~10^7 m^{-3}) and type A and type B concentrations are within the same order of magnitude. Furthermore, Perring et al. (2015) have shown type B particles constitute a considerable fraction of the total supermicron particles across the United States, being ~15% and ~25% over (altitude >100m) the Southeastern US and Southwestern US, respectively. Total particle and NON-FBAP size distributions in Figure 3c peaked at ~1µm. Similarly, types A, B, AB size distributions (Figure 3d) peaked close to 1µm showing that interferences by non-biological particles cannot be rule out. However, ABC type size distribution (red line, Figure 3d) is dominated by 3-5µm particles and ABC type particles may have come from a different source to other FBAP types as they get enhanced after rain events (e.g. 4/14; Table 1). Yu et al. (2016) also observed 4-6µm ABC type particles in the highly polluted Nanjing, China, but ABC type bimodal size distributions showed a peak between 1-2µm and a second peak between 4-6µm. In addition, ABC type number fractions in Nanjing, China correlated to black carbon mass fractions suggesting a considerable influence by combustion related particles and no rain events occurred during the sampling period. The difference between Metro Atlanta and Nanjing, China ABC type size distributions suggest ABC type is not influenced by combustion related particles in Metro Atlanta. Overall, results show FBAP concentration (1-5µm) ranges from 10^4 -10^5 m^{-3} in metro Atlanta and wet-ejected fungal spores concentration, detected by ABC type, can constitute up to 30% of the FBAP (1-5 µm) after rain events.

4.3 Correlation of HNA population with ABC type

A quantitative comparison between WIBS-4A total particle and FCM total particle concentrations was subsequently performed and we focused the analysis to the 1 to 5µm size range as SpinCon sampling efficiency is reduced significantly above 5µm (≤14%; Kesavan et al., 2015). WIBS-4A and FCM total particle concentrations differed by about one order of magnitude (for optical diameter, d_o, greater than 1.5µm) and particle concentration difference increased for particles with $d_o < 1.5$ µm as shown in the size distribution (geometrically averaged across the 15 SpinCon II sampling events) in Figure 4a. The largest difference between WIBS-4A and uncorrected FCM size distributions seems to be related to SpinCon II having a cutoff size close to 1µm, reducing significantly its sampling efficiency. Even with the observed difference in the magnitude of the concentrations between the two techniques, ABC type and HNA concentrations traced throughout all the sampling events and are ~~highly~~ moderately correlated ($R^2 = 0.40$, P-value = 0.016; Figure 4b) and showed similar size distributions in the 1 to 5µm range as shown in Figure S12a. HNA and ABC type were both dominated by 3-5µm particles and its seems both are detecting the same type of biological particles. In addition, AB type showed a weak correlation with HNA concentrations

(R^2 = 0.17), but their size distributions differed as type AB peaks close to ~1µm (Figure 3d). ABC is the only FBAP type showing a considerable correlation to the HNA population, and ~~bioLNA~~LNA-AT population is not correlated with any FBAP type. Overall, ABC type and HNA correlation is an important step forward to better understand the effectiveness of WIBS-4A FBAP categories to provide speciated PBAP concentrations in urban areas. ABC type particles have shown substantial concentrations (10^4-10^5 m^{-3}; Perring et al., 2015; Ziemba et al., 2016) across the US. The highest ABC fraction of the total FBAP was observed in Panhandle, Florida during an airborne study among multiple environments studied using WIBS-4A to sample from the California coast to central Florida, suggesting ABC type particles are ubiquitous in the US (Perring et al., 2015). Previous studies (Healy et al., 2014, Huffman et al., 2013) have shown correlations between LIF technology (e.g. WIBS-4 and UV-APS) fluorescence channels and fungal spores number concentrations, especially during fungal spores invigoration after rain events. Healy et al. (2014) used WIBS-4 in Killarney National Park, Ireland (e.g. high vegetative rural area) finding correlations between channel B (FL2; R^2 = 0.29) and channel C (FL3; R^2 = 0.38) concentrations and fungal spores concentrations (collected by Sporewatch impactor and quantified by microscopy). However, now for the first time FCM HNA population have shown a correlation with WIBS-4A ABC type and suggests ABC type category detects ~~well~~wet actively ejected fungal spores in Metro Atlanta (e.g. urban area). In addition, recent WIBS-4A experiments using pure cultures have shown ABC type detects well several fungal spores (e.g. *Aspergillus Versicolor* & *Botrytis spp*.) and small pollen grains, but detection may vary across instruments (Hernandez et al., 2016).

FCM concentrations were corrected based on correction factors (CF) calculated upon the comparison of ABC and HNA size distributions (1 to 5µm) for each sampling event given (1) ABC type and HNA population similar size distributions and number concentrations (1 to 5µm) correlation, and, (2) WIBS-4A provides us representative concentrations of airborne particle concentrations in Metro Atlanta after sampling losses being corrected (Section 3.2). Concentration correction factors were determined for each sampling episode by taking the quotient of ABC type to HNA concentrations over the 1-5µm size range. The resulting size-dependent correction factor (Figure S12b) was then applied to the FCM size distributions, giving the "corrected FCM" bioaerosol data (between 1 and 5 µm). Figure 4a shows that the corrected FCM total particle average size distribution traces WIBS-4A size distribution, allowing us to correct for SpinCon II low collection efficiency and to better constrain the magnitude of FCM concentrations. Our approach to calculate the estimated collection efficiency (ECE) considers all the processes that affect the concentration of PBAP, from collection to final quantification in the FCM. Figure S12b compares Kesavan et al. (2015) collection efficiencies determined for SpinCon I and the estimated collection efficiency calculated upon the CF calculation (ECE = 1/CF) and shows the ECE of the SpinCon II is lower that Kesavan et al. (2015) below 3µm and performs better for particles above 3µm, but above

Formatted: Font: Italic

Formatted: Font: Italic

3µm Kesavan et al (2015) collection efficiency is within the uncertainty of our calculations. Our lower ECE values (Figure S12b) for particles below 3µm can be related to SpinCon sampling time as Kesavan et al. (2015) experiment were conducted in a short period of time (e.g. 10-15 min) and ours took place for 4 ~~hr.~~h The main mechanisms leading to below 3µm particle losses could be their re-~~arosolization~~aerosolization over time being lost through the blower exhaust of the SpinCon II (Figure 1). Also, coagulation of small particles over time can not be rule out, but future work is needs to study it.

4.4 PBAP populations after collection/detection corrections

After correction through the application of the ABC correction factors, FCM total particle concentrations (1 to 5µm avg.: $5.5\times10^5 \pm 5.1\times10^5$ m^{-3}; Figure 5a) are within the same order of magnitude as WIBS-4A concentrations (1 to 5µm avg.: $5.4\times10^5 \pm 2.9\times10^5$ m^{-3}; Figure 3a), and continue to exhibit substantial variability. The HNA (e.g. fungal spores) population showed a substantial invigoration during three sampling events (4/7, 4/14, 4/15; Figure 5a and 5b). To better understand the role of meteorology on PBAP composition, the PBAP samples were classified into four regimes based on the average diurnal relative humidity and ambient temperature, with T= 18 °C (65 °F) to differentiate between warm and cold days, and, RH = 70% to differentiate between humid and dry days. The temperature and RH threshold values were chosen based on the observations and understanding that a combination of temperature and RH within these threshold values can significantly impact bioaerosol composition. For instance, humid and warm conditions~~-~~ may lead to the invigoration of fungal spores by wet ejection from plants (Ingold, 1971), on contrary, PBAP will get stressed when exposed to warm and dry conditions. The sampling times, RH, ambient temperature and meteorological categories of each SpinCon II sample is presented in Table 1.

Humid and warm days (4/7, 4/14 and 4/15; light green shaded areas in Figure 5a) were characterized by well-defined HNA and ~~bioLNA~~LNA-AT populations. These sampling episodes had the highest average HNA (fungal spore) concentration ($4.0\times 10^4 \pm 1.3\times10^4$ m^{-3}) among the four meteorological regimes and during these sampling events HNA constituted ≥ 77 % of the total PBAP. Among the humid and warm days (Figure 5a and 5b), average ~~bioLNA~~LNA-AT, HNA and "unclassified" bioaerosol compositions were 6.1%, 84.0% and 9.9%, respectively of the total PBAP number. Also, the humid and warm days occurred after rain events, which can be linked directly to the strong fungal spore invigoration (Huffman et al., 2013). Before sampling, early morning precipitation occurred during 4/14 and 4/15, as well as during the night of 4/6. Precipitation did not occur during sampling in any of the humid and warm days. The FCM results (Figure S15a-c) that display the PBAP population between 4/7 and 4/9 show a disappearance of the (HNA) fungal spore population during the transition from a "humid and warm" day (4/7) to a "dry and warm" day (4/9). Figure 5b shows how the HNA contribution to the total PBAP goes down on 4/8 when RH decreases

and is undetected on 4/9. Furthermore, Figure 6a-c shows FL1 vs. SSC-A plots for 4/14 to 4/16 consecutive sampling periods, where a marked increase in the ~~bioLNA~~LNA-AT concentration from 4/15 to 4/16 goes together with a striking decrease in the HNA concentration. HNA fraction went down from 92.0~~.5~~% to 34.1% of the total PBAP and ~~bioLNA~~LNA-AT concentration went up from 3.8×10^3 m^{-3} to 2.9×10^4 m^{-3}. Humid and Warm days had the lowest averaged PBAP concentration ($4.6 \times 10^4 \pm 9.8 \times 10^3$ m^{-3} in the 1 to 5µm range) among the four meteorological regimes, a possible effect of the bioaerosols being lost by wet scavenging, resulting in the enhancement of fungal spore contribution to the total PBAP number concentrations. The unclassified biological particles concentration also showed its lowest contribution (2.9×10^3 m^{-3}; 9.9%) to the total PBAP number concentration during these events, when the HNA and LNA populations are best identified by the 2% contour plots.

Cold and humid days (4/16 and 4/29; light yellow shaded areas in Figure 5a) also showed well-defined HNA population, and HNA contributed on average to 29.5 ± 6.5 % of the total PBAP concentration (1 to 5µm). On 4/16 drizzling took place by the end of the sampling period, but no accumulated rainfall was measured by the meteorological station. However, on 4/29, accumulated rainfall averaged 0.04in. from 11:55 AM to 2:20 PM (Figure S21). The similar HNA concentration between "Humid and Warm" and "Humid and Cold" days seen in Figure 5a and the lower contribution of HNA to the total PBAP during the "Humid and Cold" days may be linked to previously suggested bacteria emissions by droplet soil impaction during rain events (Joung et al., 2017). Bacteria emission by soil impaction can increases airborne ~~bioLNA~~LNA-AT concentration and HNA (fungal spores) will have a lower contribution to the total PBAP even when the fungal spore concentration is high during rain events. Both cold and humid days showed a considerable difference in ~~bioLNA~~LNA-AT contributions to the total PBAP concentration. On 4/16 and 4/29 ~~bioLNA~~LNA-AT constituted 45.2% and 65.3% of the total PBAP concentration, respectively (Figure 5b). The difference in the ~~bioLNA~~LNA-AT contribution to the total PBAP can be linked to the intensity of precipitation, as it shapes the composition (e.g. size and types) of microbes suspended in the atmosphere during the different stages of a rainfall (e.g. before, on set, during and after a rainfall; Yue et al., 2016).

Six of the fifteen sampling days were classified as warm and dry (4/8, 4/9, 4/22, 5/13, 5/14, 5/15; light orange shaded areas in Figure 5a) and it did not rain before or during any of these days (Table 1). During warm and dry days, HNA had the lowest averaged concentration ($8.7\times10^3 \pm 1.2\times10^4$ m^{-3}) among the four meteorological categories. In addition, during three dry and warm days (4/9, 4/22 and 5/15) the HNA population was undetected. This behavior can be related to the fact that high RH drives fungal spore emissions by wet ejection, but soil wetness could also affect emissions because the HNA population was detected in other warm and dry days with comparable RH (Huffman et al., 2013; Gosselin et al., 2016). The air mass trajectories reaching Atlanta during each sampling event could also affect the biological particles

composition. For example, on 4/22, when the HNA was undetected, the 500m and 100m 72 h backward air mass trajectories reaching Atlanta came from the NW (US/Canada border) at high altitudes and do not spend more than 24h near surface. This air mass could affect bioaerosol composition with minimal influence from local bioaerosol emissions. However, the enhancement or the depletion of the HNA population have not been linked to specific air masses trajectories. Besides meteorology, two main hypotheses could explain the observed behavior in the HNA population, previously stated by Bouvier et al., 2007 to understand HNA and LNA populations in aquatic environments, but also applicable to airborne microorganisms. First, microbes might begin in the HNA population upon aerosolization and then move to the LNA upon death or inactivity. Second, the HNA and LNA populations may contain completely different microbial taxa and have different organisms in each population. If the first hypothesis occurs, we expect to see a covariance of the HNA and LNA FCM parameters (e.g. FSC-A, SSC-A and FL1-A intensities), and observe a gradual decrease in the FL1-A intensity of the HNA population to the FL1-A values observed by particles in the LNA population, which is not seen. Although our results suggest the HNA and LNA are two distinctive populations, further studies will have to take place to sort and directly study the DNA sequences of each population in order to prove the second hypothesis. HNA population behavior may also consist of a combination of both hypotheses. Overall, warm and dry days prevail during springtime in Atlanta and ~~bioLNA~~LNA-AT contribution (avg.: $3.4\times10^4 \pm 2.5 \times10^4$ m^{-3}) may represent the bioaerosol background of Atlanta.

Four of the fifteen sampling days (4/21, 4/23, 4/28 and 4/30; light blue shaded areas in Figure 5a) were characterized by cold and dry conditions (Table 1). PBAP were dominated by ~~bioLNA~~LNA-AT during these events, as can see in Figure 7a-c, where LNA population are the dominant contributors to PBAP number. HNA population was diminished in Figure 7a (4/21) & Figure 7c (4/23) during cold and dry days and disappeared in Figure 7b during a warm and dry day. Overall, HNA was detected during cold and dry days, but showed lower contributions to the total PBAP number concentration than humid days. Among cold and dry days, the PBAP population (1 to 5 µm) was composed on average of 72.6 ± 10.1% ~~bioLNA~~LNA-AT and 16.5 ± 8.2% HNA. Cold and dry days had on average the highest ~~bioLNA~~LNA-AT ($5.3\times10^4 \pm 1.8\times10^4$ m^{-3}) and total PBAP ($7.3\times10^4 \pm 2.0\times10^4$ m^{-3}) number concentrations (1 to 5µm) among the four meteorological categories, reaching the PBAP maximum concentration on 4/23 (Figure 5a).

4.5 PBAP day-to-day variability in Metro Atlanta: FCM vs. WIBS

Although WIBS and FCM possess different methodologies, they show similar trends providing a good understanding of the daily variability of PBAP in Metro Atlanta. FCM PBAP fraction (1 to 5µm) ranges from 3.8% to 69.2% of the total particles and the highest PBAP fraction (69.2%) and HNA

Formatted: Font: Bold, Font color: Auto

concentration is observed on 4/14 ($5.25\times10^4 \pm 5.89\times10^3$ m^{-3}). The total FBAP fraction (1 to 5µm) ranges from 16% to 43%, but it reaches its maximum on 4/15. However, ABC fraction of the total WIBS particle concentration ranges from 1.3% to 9.2% and it reaches its maximum on 4/14. Even when the magnitudes of the PBAP and FBAP fractions differ on average by a factor of ~ 2 throughout the sampling period, both techniques agree an enhancement in the total biological particles takes place between 4/14 to 4/16. Given the uncertainty of the two methodologies, it is remarkable that there is such agreement between WIBS and FCM results.

Among the four meteorological categories, humid and warm days characterize for showing the highest HNA, A type, AB type and ABC type concentrations suggesting that A and AB types may also be related to wet-ejected fungal spores in Metro Atlanta; this possibly explains why the ABC fraction of the total FBAP in 4/7 is not as high as on 4/14 and 4/15 (Figure 3b), and differs with the behavior observed by the HNA population on 4/7. The ~~bioLNA~~LNA-AT population does not show a correlation to any specific FBAP type and shows it highest concentrations during dry and cold days. In addition, ~~bioLNA~~LNA-AT concentrations are anticorrelated with type B concentrations (Figure S19, correlation coefficient, r = -0.59; R^2 =0.30) during dry (both cold and warm) days, when ~~bioLNA~~LNA-AT dominates the total PBAP concentration. Given that type B particles have been previously correlated to abiotic particles (e.g. black carbon) in urban environments (Yue et al., 2017), ~~bioLNA~~LNA-AT and type B anticorrelation suggests that ~~bioLNA~~LNA-AT particles may in fact represent a heterogeneous bioaerosol population. That ~~bioLNA~~LNA-AT is not correlated with any FBAP type gives rise to two possibilities: (1) if ~~bioLNA~~LNA-AT population is mainly composed of bacteria or agglomerated bacteria, then it is possible that they are detected by multiple FBAP types and is not attributed specifically to one of them; (2) the intrinsic fluorescence of ~~bioLNA~~LNA-AT particles is too low and a high fraction of them is abiotic. It is challenging to determine what PBAP types each WIBS FBAP type is mainly detecting. Based on WIBS-4A results in Metro Atlanta, ABC type detects wet-ejected fungal spores, but still unclear what PBAP types are detect by the other FBAP types or if they just capture a high fraction of non-biological particles. FBAP types and WIBS total particles correlations in Figure S17 show all FBAP types are correlated to WIBS total particles, but ABC and AB types show the lowest correlations (type AB: R^2 =0.101; type ABC: R^2 = 0.1266).

Figure 8 shows FCM total PBAP (black line), ABC type (light green), FL1(Channel A; dark green line) and total FBAP (blue line) concentrations, where the FL1 concentration ([FL1]) constitutes the sum of the number concentrations of types A, AB, AC, and ABC ([FL1] = [A] + [AB] + [AC] + [ABC]; Gabey et al., 2011; Healy et al., 2014). Throughout the April-May 2015 sampling events, total PBAP concentrations (1 to 5µm) were mainly constrained between the FL1 and ABC type concentrations suggesting FL1 and ABC type represent the upper and lower bound PBAP concentrations in Metro Atlanta,

respectively. It also important to highlight that FCM PBAP concentrations are closer to the ABC type concentrations before April 16 when the HNA population dominates, but then after April 16 FCM PBAP concentrations are closer to FL1 concentrations when ~~bioLNA~~LNA-AT starts to dominate the total PBAP concentration. In addition, Figure 8 shows that total FBAP (sum of type A, B, C, AB, AC, ABC) exceeds the (corrected) PBAP concentrations in Metro Atlanta.

5. Conclusions

In this study we presented the development and testing of an effective FCM protocol to identify and quantify bioaerosol populations. The FCM protocol, designed to constrain any particle accumulation due to cleaning or by fluid supplies, successfully quantified the day-to-day variability of bioaerosols in the Atlanta Metro area. It is the first FCM study to detect well-defined LNA (low nucleic acid) and HNA (high nucleic acid) atmospheric biological populations under different meteorological scenarios. FCM results show dynamic bioaerosol populations in Atlanta leading to a 84.0% of HNA (wet-ejected fungal spores) and 6.1% ~~bioLNA~~LNA-AT contribution to the PBAP number (1 to 5µm range), respectively, during humid and warm days after rain events. However, ~~bioLNA~~LNA-AT dominates warm and cold dry days, constituting 72% of the PBAP number concentration.

WIBS-4A and SpinCon II collocated sampling showed that the HNA and ABC type concentrations are well correlated (R^2=0.40) and display similar size ~~distribution.~~distributions. We therefore conclude that both instruments detect the same particles, and used empirical collection/detection efficiency factors to correct the FCM size distributions and concentrations in the 1 to 5µm diameter range. WIBS-4A and FCM results suggest Metro Atlanta PBAP concentrations range between 10^4 - 10^5 m^{-3} (1 to 5µm) and they can constitute a substantial fraction of coarse mode particle concentration (WIBS-4A: 43%; FCM: 69%), comparable to the PBAP coarse mode fraction in highly vegetated environments. The FCM ~~bioLNA~~LNA-AT population, possibly containing bacterial cells, did not correlate to any FBAP type. The fact that the ~~bioLNA~~LNA-AT population is not correlated with a specific FBAP type suggests it may be particularly challenging to use LIF techniques to distinguish bioaerosols with low intrinsic autofluorescence from non-biological particles, especially given the heterogeneities introduced by the large biodiversity of airborne microbes. The possible influence of abiotic particles in the ~~bioLNA~~LNA-AT population can also explain the lack of correlation between ~~bioLNA~~LNA-AT and FBAP types given that the FCM threshold approach does not ensure total exclusion of abiotic particles. In addition, the unspecific binding of SYTO-13 to abiotic particles cannot be ruled out in the ~~bioLNA~~LNA-AT population. FCM comparison between atmospheric and pure culture samples showed lower SYTO-13 fluorescence intensities in the atmospheric samples and suggests a degradation in the genetic material of PBAP, possibly caused by the limited nutrients and strong

stress prevailing in the atmosphere, which further challenge the ability of LIF to distinguish ~~bioLNA~~LNA-AT.

In summary, this study have shown for the first time that FCM can effectively identify, quantify and study the daily variability of heterogeneous PBAP populations (e.g. HNA, ~~bioLNA~~LNA-AT and pollen) with different genetic material content in an urban environment to the degree of quantitatively correlate FCM HNA to WIBS-4A ABC type number concentrations and better understand wet-ejected fungal spores enhancement after rain events. Furthermore, FCM and WIBS-4A results show bacterial cells detection and quantification still a challenging task for LIF technology as well as for FCM, pointing to the need of concurrent complementary chemometric or molecular biology measurements for unambigious quantification, given the complexity involved to minimize abiotic interferences, and to the heterogenicity of the atmospheric samples.

Acknowledgments

We acknowledge support from a Georgia Power Faculty Scholar chair, a Cullen-Peck Faculty Fellowship, a Dreyfus Foundation Postdoctoral Fellowship in Environmental Chemistry, NASA, ~~and~~ a NASA Earth System Science Fellowship (grant no. 80NSSC17K0434). AN acknowledges support from the project PyroTRACH (ERC-2016-COG) funded from H2020-EU.1.1. - Excellent Science - European Research Council (ERC), project ID 726165. We also thank Prof. Rodney Weber for helpful suggestions on the SpinCon II flow calibration.

References

Amato, P., Joly, M., Schaupp, C., Attard, E., Möhler, O., Morris, C. E., Brunet, Y., and Delort, A. M.: Survival and ice nucleation activity of bacteria as aerosols in a cloud simulation chamber, Atmospheric Chemistry and Physics Discussions, 15, 4055-4082, 10.5194/acpd-15-4055-2015, 2015.

~~Atkinson, R. W., Strachan, D. P., Anderson, H. R., Hajat, S., and Emberlin, J.: Temporal associations between daily counts of fungal spores and asthma exacerbations, Occup Environ Med, 63, 580-590, 10.1136/oem.2005.024448, 2006.~~

Augustin, S., Hartmann, S., Pummer, B., Grothe, H., Niedermeier, D., Clauss, T., Voigtländer, J., Tomsche, L., Wex, H., and Stratmann, F.: Immersion freezing of birch pollen washing water, Atmospheric Chemistry and Physics Discussions, 12, 32911-32943, 10.5194/acpd-12-32911-2012, 2012.

Bacsi, A., Choudhury, B. K., Dharajiya, N., Sur, S., and Boldogh, I.: Subpollen particles: carriers of allergenic proteins and oxidases, J Allergy Clin Immunol, 118, 844-850, 10.1016/j.jaci.2006.07.006, 2006.

Baillie, L., and Read, T. D.: Bacillus anthracis, a bug with attitude!, Current Opinion in Microbiology, 4, 78-81, https://doi.org/10.1016/S1369-5274(00)00168-5, 2001.

Bauer, H., Claeys, M., Vermeylen, R., Schueller, E., Weinke, G., Berger, A., and Puxbaum, H.: Arabitol and mannitol as tracers for the quantification of airborne fungal spores, Atmospheric Environment, 42, 588-593, 10.1016/j.atmosenv.2007.10.013, 2008.

Bauer, H., Schueller, E., Weinke, G., Berger, A., Hitzenberger, R., Marr, I. L., and Puxbaum, H.: Significant contributions of fungal spores to the organic carbon and to the aerosol mass balance of the urban atmospheric aerosol, Atmospheric Environment, 42, 5542-5549, 10.1016/j.atmosenv.2008.03.019, 2008.

Bochdansky, A. B., Clouse, M. A., and Herndl, G. J.: Eukaryotic microbes, principally fungi and labyrinthulomycetes, dominate biomass on bathypelagic marine snow, The Isme Journal, 11, 362, 10.1038/ismej.2016.113, 2016.

Bouvier, T., Del Giorgio, P. A., and Gasol, J. M.: A comparative study of the cytometric characteristics of high and low nucleic-acid bacterioplankton cells from different aquatic ecosystems, Environ Microbiol, 9, 2050-2066, 10.1111/j.1462-2920.2007.01321.x, 2007.

Burrows, S. M., ~~Bowers, R. M., McLetchie, S., Knight, R., and Fierer, N.: Spatial variability in airborne bacterial communities across land-use types and their relationship to the bacterial communities of potential source environments, ISME J, 5, 601-612, 10.1038/ismej.2010.167, 2011.~~

Elbert, W., Lawrence, M. G., and Pöschl, U.: Bacteria in the global atmosphere – Part 1: Review and synthesis of literature data for different ecosystems, Atmos. Chem. Phys., 9, 9263-9280, https://doi.org/10.5194/acp-9-9263-2009, 2009.

Chen, P. S., and Li, C. S.: Bioaerosol characterization by flow cytometry with fluorochrome, J Environ Monit, 7, 950-959, 10.1039/b505224f, 2005.

Chi, M.-C., and Li, C.-S.: Fluorochrome in Monitoring Atmospheric Bioaerosols and Correlations with Meteorological Factors and Air Pollutants, Aerosol Science and Technology, 41, 672-678, 10.1080/02786820701383181, 2007.

Comas-Riu, J. and Vives-Rego, J. (2002), Cytometric monitoring of growth, sporogenesis and spore cell sorting in *Paenibacillus polymyxa* (formerly *Bacillus polymyxa*). Journal of Applied Microbiology, 92: 475-481. doi:10.1046/j.1365-2672.2002.01549.x

Crawford, I., Robinson, N. H., Flynn, M. J., Foot, V. E., Gallagher, M. W., Huffman, J. A., Stanley, W. R., and Kaye, P. H.: Characterization of bioaerosol emissions from a Colorado pine forest: results from the BEACHON-RoMBAS experiment, Atmospheric Chemistry and Physics Discussions, 14, 2499-2552, 10.5194/acpd-14-2499-2014, 2014.

Darrow, L. A., Hess, J., Rogers, C. A., Tolbert, P. E., Klein, M., and Sarnat, S. E.: Ambient pollen concentrations and emergency department visits for asthma and wheeze, Journal of Allergy and Clinical Immunology, 130, 630-638.e634, https://doi.org/10.1016/j.jaci.2012.06.020, 2012.

DeLeon-Rodriguez, N., Terry L. Lathem, Luis M. Rodriguez-R, James M. Barazesh, Bruce E. Anderson, Andreas J. Beyersdorf, Luke D. Ziemba, Michael Bergin, Athanasios Nenes, and Konstantinos T. Konstantinidis,: Microbiome of the upper troposphere: Species composition and prevalence, effects of tropical storms, and atmospheric implications, Proceedings of the National Academy of Sciences 110, 2575-2580, 2013.

DeLeon-Rodriguez, N.: Microbes in the atmosphere: prevalence, species composition, and relevance to cloud formation School of Biology Georgia Institute of Technology, 129 pp., (http://hdl.handle.net/1853/55517), 2015.

Delort, A.-M., and Amato, P.: Microbiology of aerosols, pp.167-168, 2018.

Després, V. R., Alex Huffman, J., Burrows, S. M., Hoose, C., Safatov, A. S., Buryak, G., Fröhlich-Nowoisky, J., Elbert, W., Andreae, M. O., Pöschl, U., and Jaenicke, R.: Primary biological aerosol particles in the atmosphere: a review, Tellus B, 64, 10.3402/tellusb.v64i0.15598, 2012.

Díaz, M., Herrero, M., García, L. A., and Quirós, C.: Application of flow cytometry to industrial microbial bioprocesses, Biochemical Engineering Journal, 48, 385-407, https://doi.org/10.1016/j.bej.2009.07.013, 2010.

Eckenrode, H. M., Jen, S.-H., Han, J., Yeh, A.-G., and Dai, H.-L.: Adsorption of a Cationic Dye Molecule on Polystyrene Microspheres in Colloids: Effect of Surface Charge and Composition Probed by Second Harmonic Generation, The Journal of Physical Chemistry B, 109, 4646-4653, 10.1021/jp045610q, 2005.

Elbert, W., Taylor, P. E., Andreae, M. O., & Pöschl, U.: Contribution of fungi to primary biogenic aerosols in the atmosphere: wet and dry discharged spores, carbohydrates, and inorganic ions., Atmospheric Chemistry and Physics, 7, 4569-4588, 2007.

~~Fennelly, J. M., Sewell, G., Prentice, B. M., O'Connor, J. D., and Sodeau, R. J.: Review: The Use of Real-Time Fluorescence Instrumentation to Monitor Ambient Primary Biological Aerosol Particles (PBAP), Atmosphere, 9, 10.3390/atmos9010001, 2018.~~

Fröhlich-Nowoisky, J., Kampf, C. J., Weber, B., Huffman, J. A., Pöhlker, C., Andreae, M. O., Lang-Yona, N., Burrows, S. M., Gunthe, S. S., Elbert, W., Su, H., Hoor, P., Thines, E., Hoffmann, T., Després,

V. R., and Pöschl, U.: Bioaerosols in the Earth system: Climate, health, and ecosystem interactions, Atmospheric Research, 182, 346-376, http://dx.doi.org/10.1016/j.atmosres.2016.07.018, 2016.

Gabey, A. M., Gallagher, M. W., Whitehead, J., Dorsey, J. R., Kaye, P. H., and Stanley, W. R.: Measurements and comparison of primary biological aerosol above and below a tropical forest canopy using a dual channel fluorescence spectrometer, Atmospheric Chemistry and Physics, 10, 4453-4466, 10.5194/acp-10-4453-2010, 2010.

Gabey, A. M., Stanley, W. R., Gallagher, M. W., and Kaye, P. H.: The fluorescence properties of aerosol larger than 0.8 μm in urban and tropical rainforest locations, Atmospheric Chemistry and Physics, 11, 5491-5504, 10.5194/acp-11-5491-2011, 2011.

Gosselin, M. I., Rathnayake, C. M., Crawford, I., Pöhlker, C., Fröhlich-Nowoisky, J., Schmer, B., Després, V. R., Engling, G., Gallagher, M., Stone, E., Pöschl, U., and Huffman, J. A.: Fluorescent bioaerosol particle, molecular tracer, and fungal spore concentrations during dry and rainy periods in a semi-arid forest, Atmos. Chem. Phys., 16, 15165-15184, 10.5194/acp-16-15165-2016, 2016.

Goudie, A. S.: Desert dust and human health disorders, Environment International, 63, 101-113, http://dx.doi.org/10.1016/j.envint.2013.10.011, 2014.

Griffin, D. W., Kellogg, C. A., Garrison, V. H., Lisle, J. T., Borden, T. C., and Shinn, E. A.: Atmospheric microbiology in the northern Caribbean during African dust events, Aerobiologia, 19, 143-157, 10.1023/B:AERO.0000006530.32845.8d, 2003.

Grote, M., Valenta, R., and Reichelt, R.: Abortive pollen germination: A mechanism of allergen release in birch, alder, and hazel revealed by immunogold electron microscopy, J. Allergy Clin. Immun., 111, 1017–1023, doi:10.1067/mai.2003.1452, 2003.

Guarín, F. A., Abril, M. A. Q., Alvarez, A., and Fonnegra, R.: Atmospheric pollen and spore content in the urban area of the city of Medellin, Colombia, Hoehnea, 42, 9-19, 2015.

Guindulain, T., J. Comas, and J. Vives-Rego: Use of nucleic acid dyes SYTO-13, TOTO-1, and YOYO-1 in the study of Escherichia coli and marine prokaryotic populations by flow cytometry, Applied and environmental microbiology, 63, 4608 - 4611, 1997.

Harrison, R. M., Jones, A. M., Biggins, P. D. E., Pomeroy, N., Cox, C. S., Kidd, S. P., Hobman, J. L., Brown, N. L., and Beswick, A.: Climate factors influencing bacterial count in background air samples, International Journal of Biometeorology, 49, 167-178, 10.1007/s00484-004-0225-3, 2005.

Healy, D. A., Huffman, J. A., O'Connor, D. J., Pöhlker, C., Pöschl, U., and Sodeau, J. R.: Ambient measurements of biological aerosol particles near Killarney, Ireland: a comparison between real-time fluorescence and microscopy techniques, Atmos. Chem. Phys., 14, 8055-8069, 10.5194/acp-14-8055-2014, 2014.

Healy, D. A., O'Connor, D. J., and Sodeau, J. R.: Measurement of the particle counting efficiency of the "Waveband Integrated Bioaerosol Sensor" model number 4 (WIBS-4), Journal of Aerosol Science, 47, 94-99, http://dx.doi.org/10.1016/j.jaerosci.2012.01.003, 2012.

Hernandez, M., Perring, A. E., McCabe, K., Kok, G., Granger, G., and Baumgardner, D.: Chamber catalogues of optical and fluorescent signatures distinguish bioaerosol classes, Atmos. Meas. Tech., 9, 3283-3292, https://doi.org/10.5194/amt-9-3283-2016, 2016.

Hill, S. C., Mayo, M. W., and Chang, R. K.: Fluorescence of bacteria, pollens, and naturally occurring airborne particles: excitation/emission spectra, Army Research Lab Adelphi Md Computational And Information Sciences Directorate, 2009.

Hoose, C., Kristjánsson, J. E., and Burrows, S. M.: How important is biological ice nucleation in clouds on a global scale?, Environmental Research Letters, 5, 024009, 2010.

Hoose, C., and Möhler, O.: Heterogeneous ice nucleation on atmospheric aerosols: a review of results from laboratory experiments, Atmos. Chem. Phys., 12, 9817-9854, 10.5194/acp-12-9817-2012, 2012.

Huffman, J. A., B. Treutlein, and U. Pöschl: Fluorescent biological aerosol particle concentrations and size distributions measured with an Ultraviolet Aerodynamic Particle Sizer (UV-APS) in Central Europe, Atmospheric Chemistry and Physics, 10, 3215-3233, 2010.

Huffman, J. A., Prenni, A. J., DeMott, P. J., Pöhlker, C., Mason, R. H., Robinson, N. H., Fröhlich-Nowoisky, J., Tobo, Y., Després, V. R., Garcia, E., Gochis, D. J., Harris, E., Müller-Germann, I., Ruzene, C., Schmer, B., Sinha, B., Day, D. A., Andreae, M. O., Jimenez, J. L., Gallagher, M., Kreidenweis, S. M., Bertram, A. K., and Pöschl, U.: High concentrations of biological aerosol particles and ice nuclei during and after rain, Atmospheric Chemistry and Physics, 13, 6151-6164, 10.5194/acp-13-6151-2013, 2013.

Ingold, C. T.: Fungal spores. Their liberation and dispersal, Oxford, Clarendon Press., 302 pp. pp., 1971.

Joly, M., Amato, P., Sancelme, M., Vinatier, V., Abrantes, M., Deguillaume, L., and Delort, A.-M.: Survival of microbial isolates from clouds toward simulated atmospheric stress factors, Atmospheric Environment, 117, 92-98, https://doi.org/10.1016/j.atmosenv.2015.07.009, 2015.

Joung, Y. S., and Buie, C. R.: Aerosol generation by raindrop impact on soil, 6, 6083, 10.1038/ncomms7083, https://www.nature.com/articles/ncomms7083#supplementary-information, 2015.

Kesavan, J., and Sagripanti, J. L.: Evaluation criteria for bioaerosol samplers, Environ Sci Process Impacts, 17, 638-645, 10.1039/c4em00510d, 2015.

Lange, J. L. T., P S and Lynch, N: Application of flow cytometry and fluorescent in situ hybridization for assessment of exposures to airborne bacteria Appl. Environ. Microbiol. , 63, 1557-1563, 1997.

Lebaron, P., Servais, P., Agogue, H., Courties, C., and Joux, F.: Does the high nucleic acid content of individual bacterial cells allow us to discriminate between active cells and inactive cells in aquatic systems?, Appl Environ Microbiol, 67, 1775-1782, 10.1128/AEM.67.4.1775-1782.2001, 2001.

Li, D.-W., and Bryce Kendrick: A year-round study on functional relationships of airborne fungi with meteorological factors, International Journal of Biometeorology 39, 74-80, 1995.

Liang, L., Engling, G., Cheng, Y., Duan, F., Du, Z., and He, K.: Rapid detection and quantification of fungal spores in the urban atmosphere by flow cytometry, Journal of Aerosol Science, 66, 179-186, 10.1016/j.jaerosci.2013.08.013, 2013.

Lin, H., Gomez, I., and Meredith, J. C.: Pollenkit Wetting Mechanism Enables Species-Specific Tunable Pollen Adhesion, Langmuir, 29, 3012-3023, 10.1021/la305144z, 2013.

Longo, A. F., Ingall, E. D., Diaz, J. M., Oakes, M., King, L. E., Nenes, A., Mihalopoulos, N., Violaki, K., Avila, A., Benitez-Nelson, C. R., Brandes, J., McNulty, I., and Vine, D. J.: P-NEXFS analysis of aerosol

phosphorus delivered to the Mediterranean Sea, Geophysical Research Letters, 41, 4043-4049, 10.1002/2014GL060555, 2014.

~~Möhler, O., DeMott, P. J., Vali, G., & Levin, Z.: Microbiology and atmospheric processes: the role of biological particles in cloud physics., Biogeosciences, 4, 1059-1071, 2007.~~

Monier, J. M., and Lindow, S. E.: Pseudomonas syringae Responds to the Environment on Leaves by Cell Size Reduction, Phytopathology, 93, 1209-1216, 10.1094/PHYTO.2003.93.10.1209, 2003.

Morris, C. E., Conen, F., Alex Huffman, J., Phillips, V., Poschl, U., and Sands, D. C.: Bioprecipitation: a feedback cycle linking earth history, ecosystem dynamics and land use through biological ice nucleators in the atmosphere, Glob Chang Biol, 20, 341-351, 10.1111/gcb.12447, 2014.

Muller, S., and Nebe-von-Caron, G.: Functional single-cell analyses: flow cytometry and cell sorting of microbial populations and communities, FEMS Microbiol Rev, 34, 554-587, 10.1111/j.1574-6976.2010.00214.x, 2010.

Myriokefalitakis, S., Nenes, A., Baker, A. R., Mihalopoulos, N., and Kanakidou, M.: Bioavailable atmospheric phosphorous supply to the global ocean: a 3-D global modeling study, Biogeosciences, 13, 6519-6543, 10.5194/bg-13-6519-2016, 2016.

Nir, R., Yisraeli, Y., Lamed, R., & Sahar, E.: Flow cytometry sorting of viable bacteria and yeasts according to beta-galactosidase activity, Applied and environmental microbiology, 56, 3861-3866, 1990.

Oliveira, M., Ribeiro, H., Delgado, J. L., and Abreu, I.: The effects of meteorological factors on airborne fungal spore concentration in two areas differing in urbanisation level, Int J Biometeorol, 53, 61-73, 10.1007/s00484-008-0191-2, 2009.

Ortiz-Martínez, Mario G., Rosa I. Rodríguez-Cotto, Mónica A. Ortiz-Rivera, Cedric W. Pluguez-Turull, and Braulio D. Jiménez-Vélez. Linking endotoxins, African dust PM10 and asthma in an urban and rural environment of Puerto Rico. *Mediators of inflammation* 2015.

~~Pérez, C. F., Gassmann, M. I., and Covi, M.: An evaluation of the airborne pollen–precipitation relationship with the superposed epoch method, Aerobiologia, 25, 313-320, 10.1007/s10453-009-9135-5, 2009.~~

Pan, Y.-L., Santarpia, J. L., Ratnesar-Shumate, S., Corson, E., Eshbaugh, J., Hill, S. C., Williamson, C. C., Coleman, M., Bare, C., and Kinahan, S.: Effects of ozone and relative humidity on fluorescence spectra of octapeptide bioaerosol particles, Journal of Quantitative Spectroscopy and Radiative Transfer, 133, 538-550, https://doi.org/10.1016/j.jqsrt.2013.09.017, 2014.

Perring, A. E., et al. (2015), Airborne observations of regional variation in fluorescent aerosol across the United States, *J. Geophys. Res. Atmos.*, 120, 1153–1170, doi:10.1002/2014JD022495.

Pöhlker, C., Huffman, J. A., Förster, J. D., and Pöschl, U.: Autofluorescence of atmospheric bioaerosols: spectral fingerprints and taxonomic trends of pollen, Atmospheric Measurement Techniques, 6, 3369-3392, 10.5194/amt-6-3369-2013, 2013.

Pöhlker, C., Huffman, J. A., and Pöschl, U.: Autofluorescence of atmospheric bioaerosols – fluorescent biomolecules and potential interferences, Atmospheric Measurement Techniques, 5, 37-71, 10.5194/amt-5-37-2012, 2012.

Pöschl, U.: Atmospheric Aerosols: Composition, Transformation, Climate and Health Effects, Angewandte Chemie International Edition, 44, 7520-7540, 10.1002/anie.200501122, 2005.

Robinson, N. H., Allan, J. D., Huffman, J. A., Kaye, P., H., Foot, V. E., and Gallagher, M.: Cluster analysis of WIBS single-particle bioaerosol data, Atmos. Meas. Tech., 6, 337-347, https://doi.org/10.5194/amt-6-337-2013, 2013.

Rödiger, S., Ruhland, M., Schmidt, C., Schröder, C., Grossmann, K., Böhm, A., Nitschke, J., Berger, I., Schimke, I., and Schierack, P.: Fluorescence Dye Adsorption Assay to Quantify Carboxyl Groups on the Surface of Poly(methyl methacrylate) Microbeads, Analytical Chemistry, 83, 3379-3385, 10.1021/ac103277s, 2011.

S.-L.Von der Weiden, F. D., and S. Borrmann: Particle Loss Calculator - a new software tool for the assessment of the performance of aerosol inlet systems, Atmospheric Measurement Techniques, 2, 479-494, 2009.

Saari, S., Reponen, T., and Keskinen, J.: Performance of Two Fluorescence-Based Real-Time Bioaerosol Detectors: BioScout vs. UVAPS, Aerosol Science and Technology, 48, 371-378, 10.1080/02786826.2013.877579, 2014.

Šantl-Temkiv, T., Amato, P., Gosewinkel, U., Thyrhaug, R., Charton, A., Chicot, B., Finster, K., Bratbak, G., and Löndahl, J.: High-Flow-Rate Impinger for the Study of Concentration, Viability, Metabolic Activity, and Ice-Nucleation Activity of Airborne Bacteria, Environmental Science & Technology, 51, 11224-11234, 10.1021/acs.est.7b01480, 2017.

Savage, N. J., Krentz, C. E., Könemann, T., Han, T. T., Mainelis, G., Pöhlker, C., and Huffman, J. A.: Systematic characterization and fluorescence threshold strategies for the wideband integrated bioaerosol sensor (WIBS) using size-resolved biological and interfering particles, Atmospheric Measurement Techniques, 10, 4279-4302, 10.5194/amt-10-4279-2017, 2017.

~~Siljamo, P., Sofiev, M., Severova, E., Ranta,~~Standaert-Vitse, A., Aliouat-Denis, C.-M., Martinez, A., Khalife, S., Pottier, M., Gantois, N., Dei-Cas, E., and Aliouat, E. M.: SYTO-13, a Viability Marker as a New Tool to Monitor In Vitro Pharmacodynamic Parameters of Anti-Pneumocystis Drugs, PLoS One, 10, e0130358-e0130358, 10.1371/journal.pone.0130358, 2015.

~~H., Kukkonen, J., Polevova, S., Kubin, E., and Minin, A.: Sources, impact and exchange of early-spring birch pollen in the Moscow region and Finland, Aerobiologia, 24, 211-230, 10.1007/s10453-008-9100-8, 2008.~~

Sullivan, S. C., Hoose, C., Kiselev, A., Leisner, T., and Nenes, A.: Initiation of secondary ice production in clouds, Atmos. Chem. Phys. Discuss., 2017, 1-22, 10.5194/acp-2017-387, 2017.

Taylor, P. E., Jacobson, K. W., House, J. M., and Glovsky, M. M.: Links between pollen, atopy and the asthma epidemic, Int Arch Allergy Immunol, 144, 162-170, 10.1159/000103230, 2007.

Toprak, E., and Schnaiter, M.: Fluorescent biological aerosol particles measured with the Waveband Integrated Bioaerosol Sensor WIBS-4: laboratory tests combined with a one year field study, Atmospheric Chemistry and Physics, 13, 225-243, 10.5194/acp-13-225-2013, 2013.

Van Dilla, M. A., Langlois, R. G., Pinkel, D., Yajko, D., & Hadley, W. K.: Bacterial characterization by flow cytometry., Science, 220, 620-622, 1983.

Wang, Y., Hammes, F., De Roy, K., Verstraete, W., and Boon, N.: Past, present and future applications of flow cytometry in aquatic microbiology, Trends Biotechnol, 28, 416-424, 10.1016/j.tibtech.2010.04.006, 2010.

Wu, Y.-H., Chan, C.-C., Rao, C. Y., Lee, C.-T., Hsu, H.-H., Chiu, Y.-H., and Chao, H. J.: Characteristics, determinants, and spatial variations of ambient fungal levels in the subtropical Taipei metropolis, Atmospheric Environment, 41, 2500-2509, 10.1016/j.atmosenv.2006.11.035, 2007.

Yu, X., Wang, Z., Zhang, M., Kuhn, U., Xie, Z., Cheng, Y., Pöschl, U., and Su, H.: Ambient measurement of fluorescent aerosol particles with a WIBS in the

Yangtze River Delta of China: potential impacts of combustion-related aerosol particles, Atmospheric Chemistry and Physics, 16, 11337-11348, 10.5194/acp-16-11337-2016, 2016.

Yue, S., Ren, H., Fan, S., Sun, Y., Wang, Z., and Fu, P.: Springtime precipitation effects on the abundance of fluorescent biological aerosol particles and HULIS in Beijing, Sci Rep, 6, 29618, 10.1038/srep29618, 2016.

Yue, S., Ren, H., Fan, S., Wei, L., Zhao, J., Bao, M., Hou, S., Zhan, J., Zhao, W., Ren, L., Kang, M., Li, L., Zhang, Y., Sun, Y., Wang, Z., and Fu, P.: High Abundance of Fluorescent Biological Aerosol Particles in Winter in Beijing, China, ACS Earth and Space Chemistry, 1, 493-502, 10.1021/acsearthspacechem.7b00062, 2017.

Zhen, H., Han, T., Fennell, D. E., and Mainelis, G.: Release of free DNA by membrane-impaired bacterial aerosols due to aerosolization and air sampling, Appl Environ Microbiol, 79, 7780-7789, 10.1128/AEM.02859-13, 2013.

Ziemba, L. D., Beyersdorf, A. J., Chen, G., Corr, C. A., Crumeyrolle, S. N., Diskin, G., Hudgins, C., Martin, R., Mikoviny, T., Moore, R., Shook, M., Thornhill, K. L., Winstead, E. L., Wisthaler, A., and Anderson, B. E.: Airborne observations of bioaerosol over the Southeast United States using a Wideband Integrated Bioaerosol Sensor, Journal of Geophysical Research: Atmospheres, 121, 8506-8524, 10.1002/2015JD024669, 2016.

Table 1: Summary of the SpinCon II sampling events, the 24 h. averaged RH, ambient temperature, the assigned meteorological category (using Section 4.4 definitions) and the corrected FCM-derived PBAP number concentration (1 to 5 µm) for each sample collected during this study.

Date (starting – ending time)	RH (%)	Temperature (°C)	Meteorological Category	PBAP Concentration (m^{-3}) 1 to 5µm diameter range
4/7/15 (11:17 - 15:17) *	70.9	21.4	Humid, Warm	9.282×10^{4}
4/8/15 (11:10 - 15:10)	53.6	24.9	Dry, Warm	5.203×10^{5}
4/9/15 (11:15 - 15:15)	53.8	25.3	Dry, Warm	1.254×10^{5}
4/14/15 (11:30 - 15:30) *	76.8	22.5	Humid, Warm	8.253×10^{4}
4/15/15 (11:40 - 15:40) *	83.6	18.9	Humid, Warm	1.234×10^{5}
4/16/15 (10:55 - 14:55)	86.3	12.5	Humid, Cold	3.399×10^{5}
4/21/15 (13:15 - 17:15)	43.2	16.6	Dry, Cold	4.741×10^{5}
4/22/15 (11:25 - 15:25)	41.2	19.0	Dry, Warm	3.351×10^{5}
4/23/15 (11:35 - 15:35)	48.1	16.8	Dry, Cold	1.708×10^{6}
4/28/15 (12:25 - 16:25)	45.3	17.0	Dry, Cold	4.899×10^{5}
4/29/15 (11:55 - 15:55) #	79.4	14.2	Humid, Cold	4.591×10^{5}
4/30/15 (12:10 - 16:10)	57.3	17.4	Dry, Cold	9.603×10^{5}
5/13/15 (10:50 - 14:50)	40.1	23.5	Dry, Warm	3.680×10^{5}
5/14/15 (11:50 - 15:50)	52.3	23.0	Dry, Warm	4.851×10^{5}
5/15/15 (10:19 - 14:19)	64.4	23.1	Dry, Warm	1.656×10^{6}

* Sampling occurred post-rain event.
# Sampling occurred during a rain event.

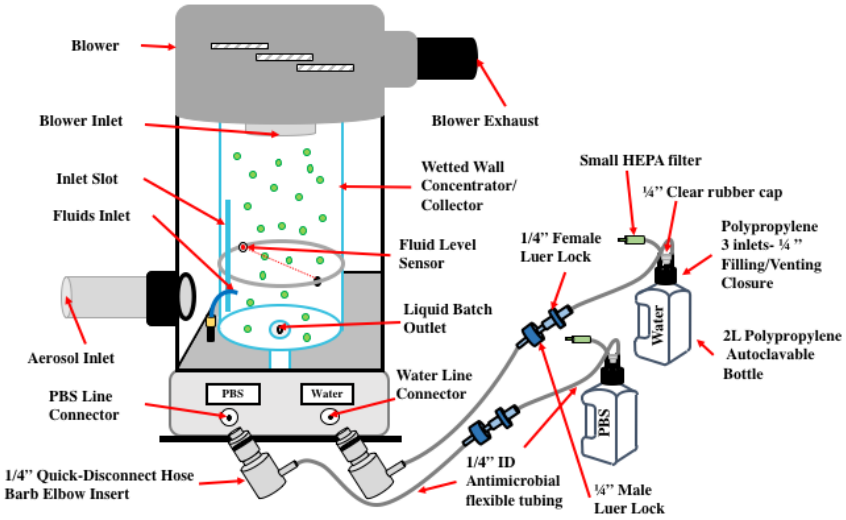

Figure 1: SpinCon II sampling setup including modified fluid supply system with anti-microbial tubing and 2L Autoclavable bottles.

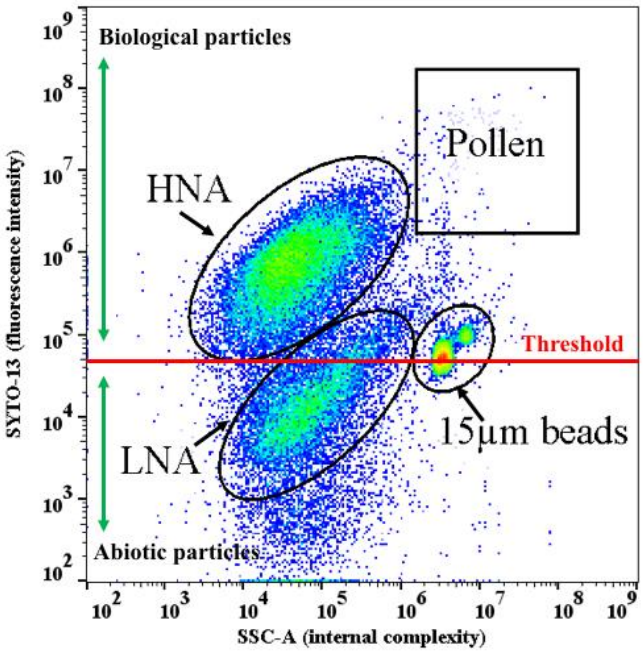
Biological particles
Pollen
HNA
Threshold
15µm beads
LNA
Abiotic particles
SYTO-13 (fluorescence intensity)
SSC-A (internal complexity)
10^2
10^3
10^4
10^5
10^6
10^7
10^8
10^9

13

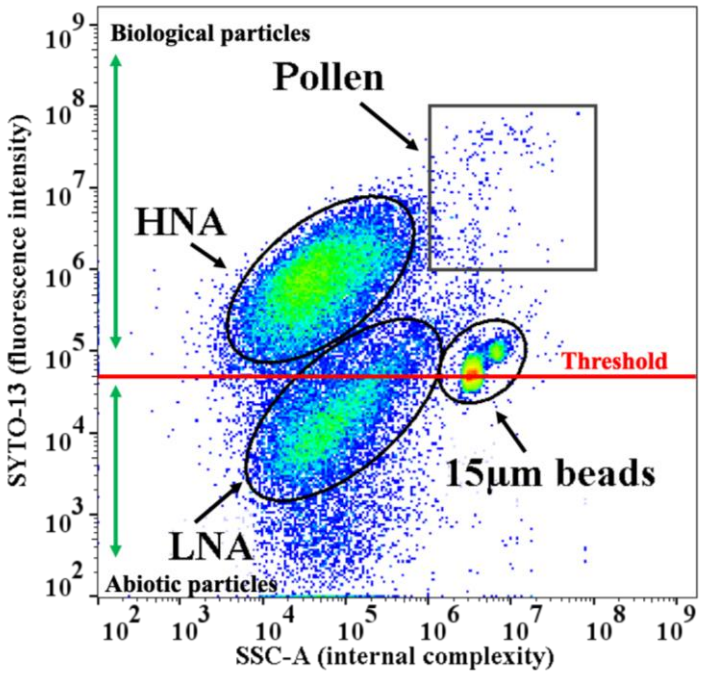

Figure 2: FL1-A vs. SSC-A plot used to identify populations in ~~collected rooftop atmospheric samples (~~the April 14, 2015 ~~4hr~~ sample~~)~~ including: the 42k threshold line in red and, abiotic particles (below threshold) and biological particles (above threshold) designated regions. In the density plot green and red zones denote the most populated regions. FL1-A in the y-axis shows the fluorescence intensity of each particle in the plot stained with SYTO-13 and SSC-A in the x-axis measures 90° light scattering, related to the internal complexity of the particles. The fraction of the LNA population above the threshold line is referred as the "~~bioLNA~~LNA-AT" population.

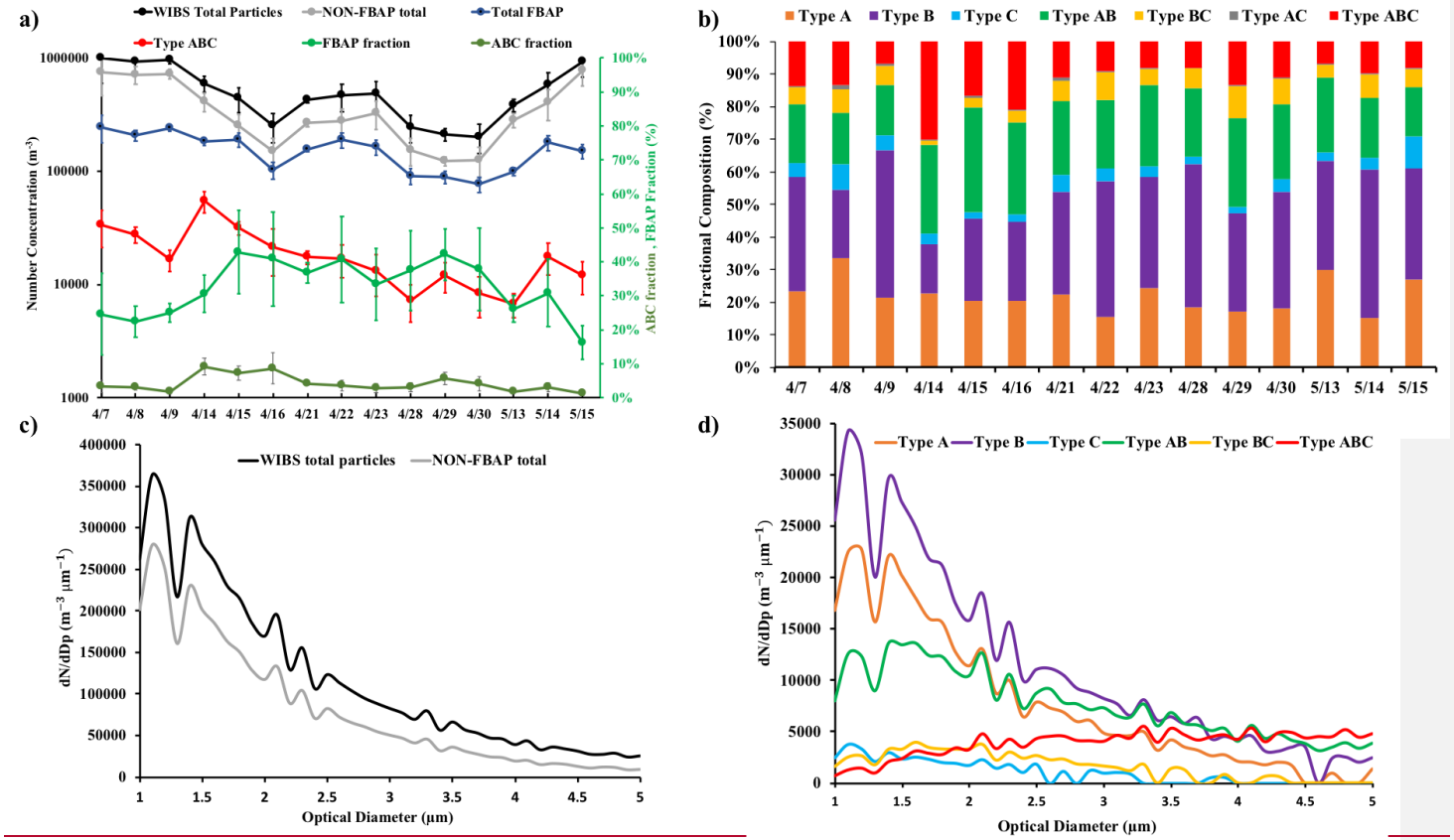
a)
WIBS Total Particles
NON-FBAP total
Total FBAP
Type ABC
FBAP fraction
ABC fraction
Number Concentration (m-3)
ABC fraction , FBAP Fraction (%)
1000000
100000
10000
1000
100%
90%
80%
70%
60%
50%
40%
30%
20%
10%
0%
4/7 4/8 4/9 4/14 4/15 4/16 4/21 4/22 4/23 4/28 4/29 4/30 5/13 5/14 5/15
b)
Type A
Type B
Type C
Type AB
Type BC
Type AC
Type ABC
Fractional Composition (%)
100%
90%
80%
70%
60%
50%
40%
30%
20%
10%
0%
4/7 4/8 4/9 4/14 4/15 4/16 4/21 4/22 4/23 4/28 4/29 4/30 5/13 5/14 5/15
c)
WIBS total particles
NON-FBAP total
dN/dDp (m-3 µm-1)
400000
350000
300000
250000
200000
150000
100000
50000
0
1 1.5 2 2.5 3 3.5 4 4.5 5
Optical Diameter (µm)
d)
Type A
Type B
Type C
Type AB
Type BC
Type ABC
dN/dDp (m-3 µm-1)
35000
30000
25000
20000
15000
10000
5000
0
1 1.5 2 2.5 3 3.5 4 4.5 5
Optical Diameter (µm)

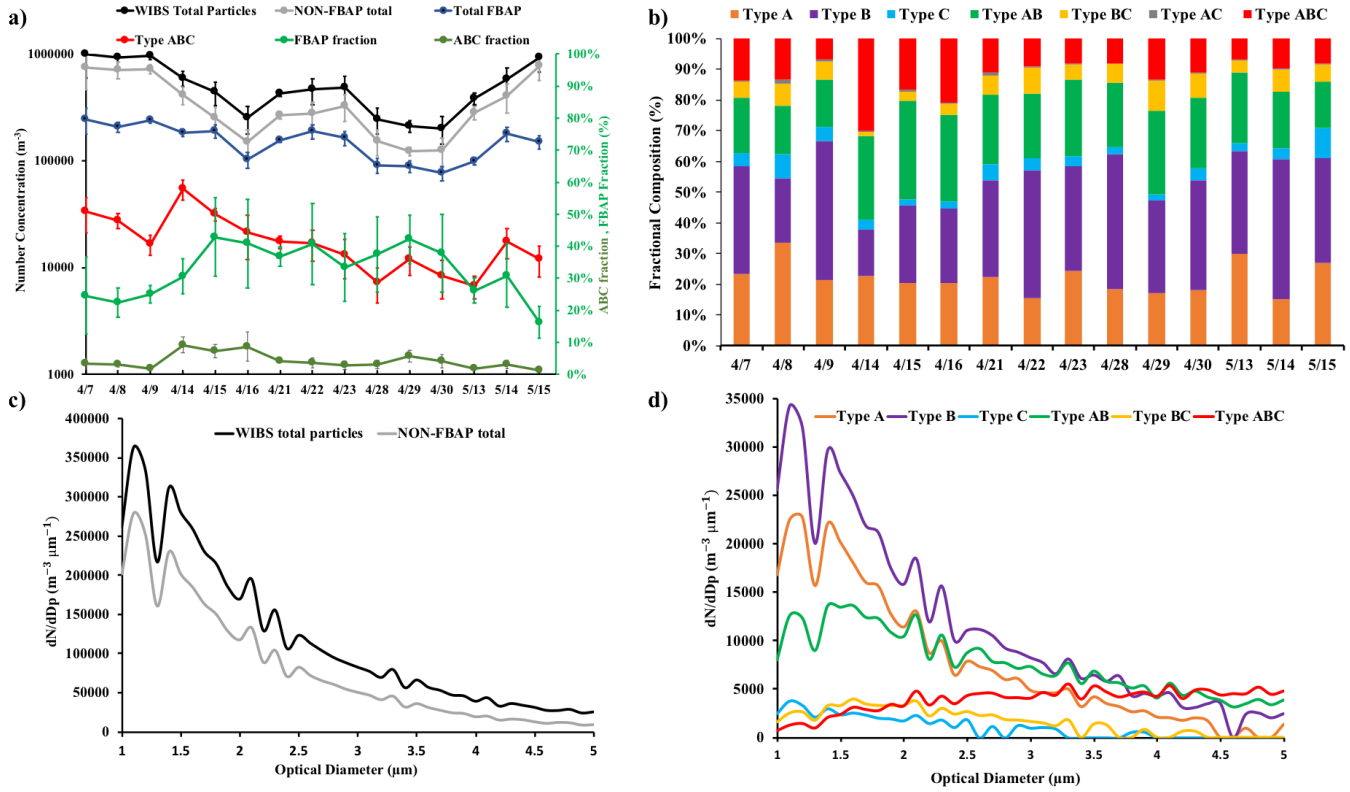

Figure 3: WIBS-4A ~~4h~~4hr (SpinCon II sampling time) averaged results of WIBS total particle, NON-FBAP, total FBAP and type ABC concentrations in the left Y-axis and ABC and FBAP fraction in the right Y-axis for each SpinCon II sampling event in (a~~) and~~); 4hr averaged FBAP types number concentration fractional composition ~~in (b); and average 1 to5µm size distributions (average of the 15 sampling events 4h average) over the 15~~ for each SpinCon II sampling ~~events of~~event in (b); 1to5µm WIBS total particles and NON-FBAP size distributions in (c) and 1to5µm size distributions for all FBAP types, except AC type in (d). AC type showed low statistics and constituted less than 1% of the total FBAP (not shown~~)~~

). Size distributions in (c) and (d) have been averaged over the 15 SpinCon II sampling events and constitute the overall size distributions during rooftop sampling events.

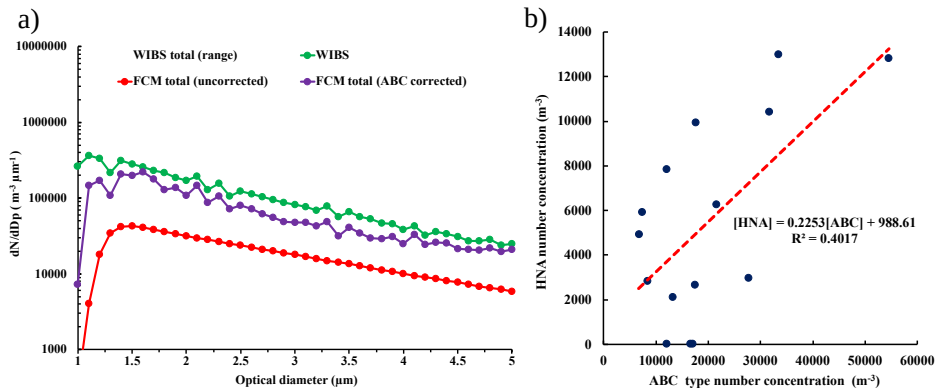

Figure 4: WIBS-4A, FCM uncorrected and FCM (ABC corrected) total particle concentration (1 to 5µm) average size distributions (geometrically averaged over the 15 SpinCon II sampling events) including WIBS range (± geometric standard deviation factor) in (a); and HNA and ABC type concentration correlation in the 1 to 5µm range in (b) including it linear correlation in red.

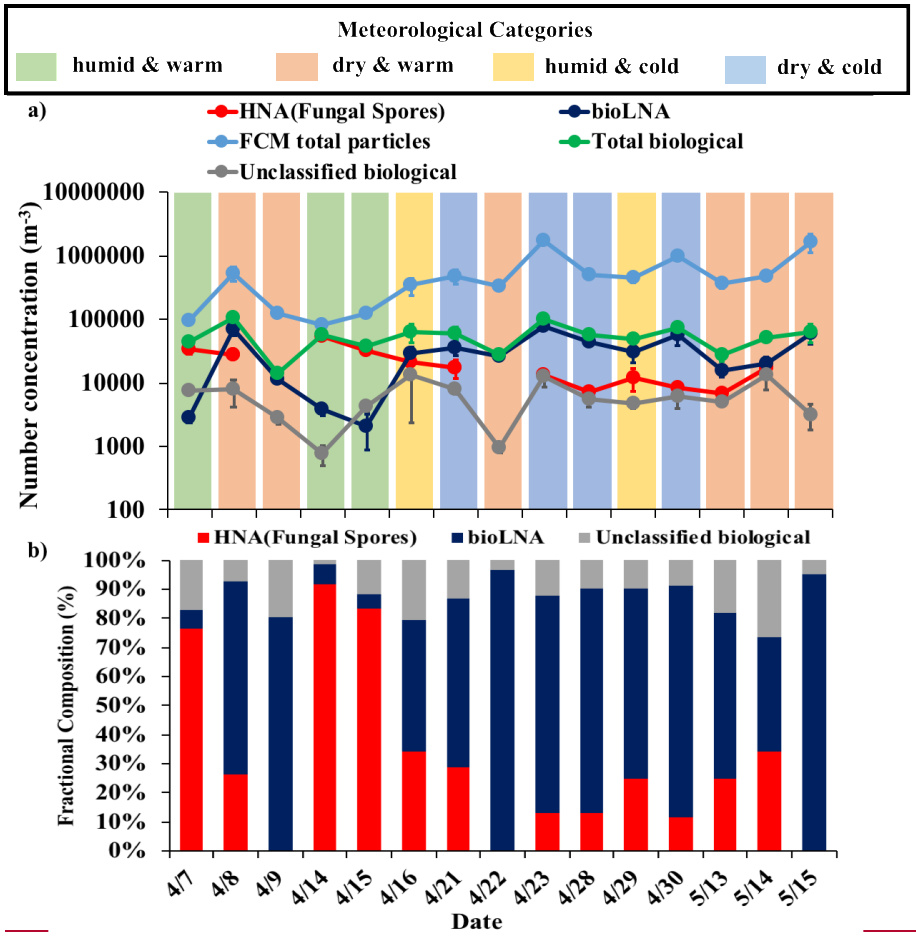
Meteorological Categories
humid & warm
dry & warm
humid & cold
dry & cold
a)
HNA(Fungal Spores)
bioLNA
FCM total particles
Total biological
Unclassified biological
Number concentration (m-3)
10000000
1000000
100000
10000
1000
100
b)
HNA(Fungal Spores)
bioLNA
Unclassified biological
Fractional Composition (%)
100%
90%
80%
70%
60%
50%
40%
30%
20%
10%
0%
4/7
4/8
4/9
4/14
4/15
4/16
4/21
4/22
4/23
4/28
4/29
4/30
5/13
5/14
5/15
Date

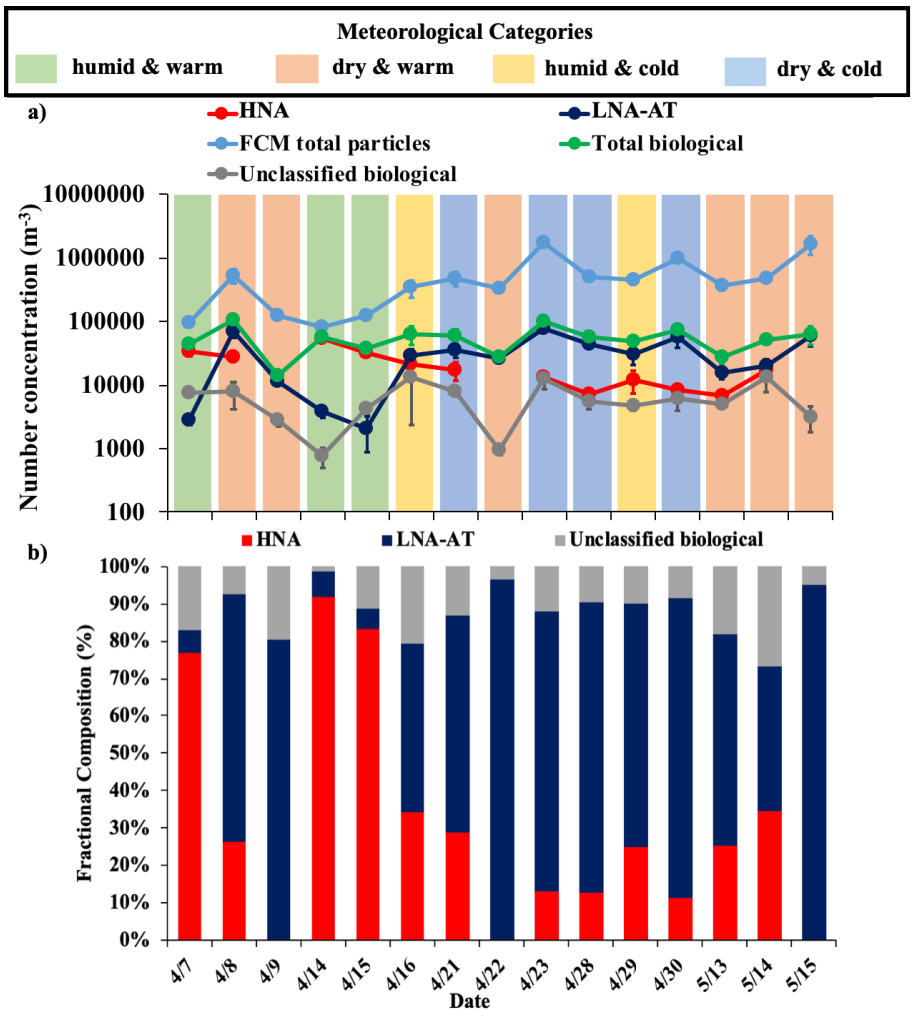

Figure 5: FCM total particle, HNA, ~~bioLNA~~LNA-AT and total PBAP number concentrations in the 1 to 5µm range highlighting the prevailing meteorological category during each sampling event in (a); HNA and ~~bioLNA~~LNA-AT number concentration fractional compositions for each sampling event in (b).

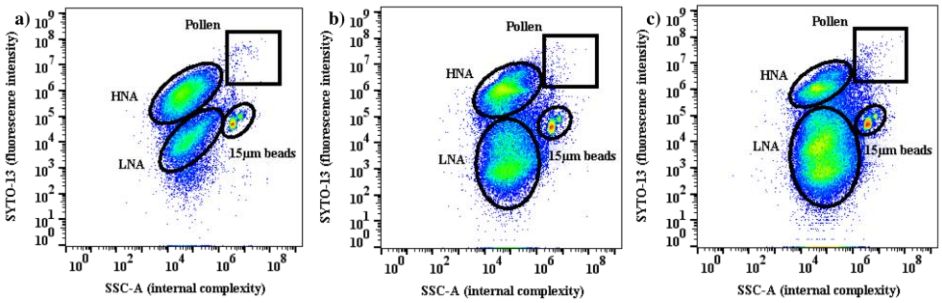

Figure 6: FL1-A vs. SSC-A FSC plots for (a) April 14, (b) April 15, and, (c) April 16. This period was characterized by a transition from humid & warm to humid & cold conditions (diurnal average RH=77%, T=22.5 ºC on 4/14; RH=84%, T=18.9 ºC on 4/15, and RH= 86%, T= 12.5 ºC on 4/16). The FCM plots during this transition period show a decrease of fungal population and an increase of the LNA population. In each population, warmer colors represent higher particle concentrations.

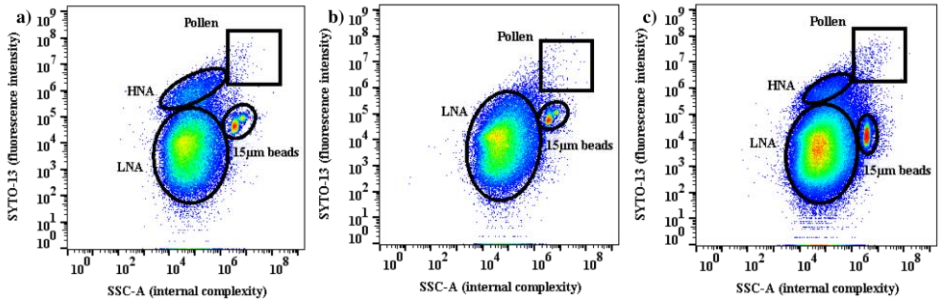

Figure 7: Similar to Figure 6, but for (a) April 21, (b) April 22, (c) April 23, which was characterized by dry and variability in temperature (diurnal average RH=43%, T=16.6 ºC on 4/21; RH=41%, T=19.0 ºC on 4/22, and, RH= 48%, T= 16.8 ºC on 4/23. Note the disappearance of the fungal spore population on the warmest day (4/22).

Formatted: Left

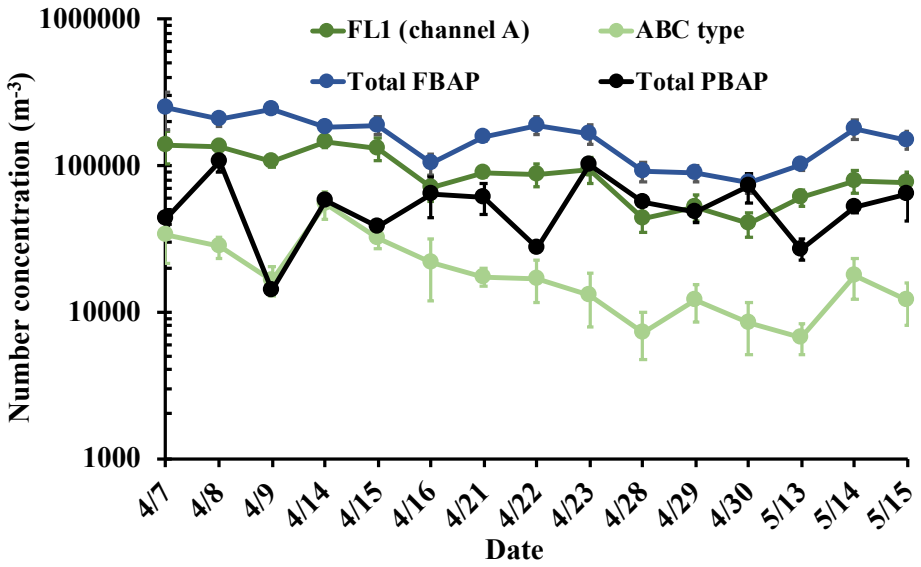

Figure 8: WIBS-4A total FBAP, FL1 and ABC type, and FCM total particle number concentrations in the 1 to 5µm range for each sampling event from April 7 to May 15, 2015.

Negron et al.,: supplementary information

Style Definition: Comment Text

SI.1 Calibration of the bioaerosol sampler flow rate

The flow rate of air sampled by the SpinCon II was calibrated with a VT100 Hotwire Thermo-anemometer (Cole Palmer Inc.), attached to a tube temporarily mounted on the sampler inlet while the instrument was in operation. Several measurements of flow velocity were taken from 3 ports (Figure S1, Holes 1-3) so that the anemometer tip was located at the center of the tube (green dot in Figure S1). The high flow rate ensures that highly turbulent conditions exist in the tube, so that the axial velocity, U, varies little in the radial direction. The volumetric flow rate, Q, is then obtained from U as:

$$Q = (\frac{\pi}{4})(ID)^2 U \quad [S1]$$

where ID is the inner diameter of the tube. The average volumetric flow rate was 478 ± 6 L min^{-1}, which represents a 6% difference to the 450 L min^{-1} flow rate reported by InnovaPrep Inc.

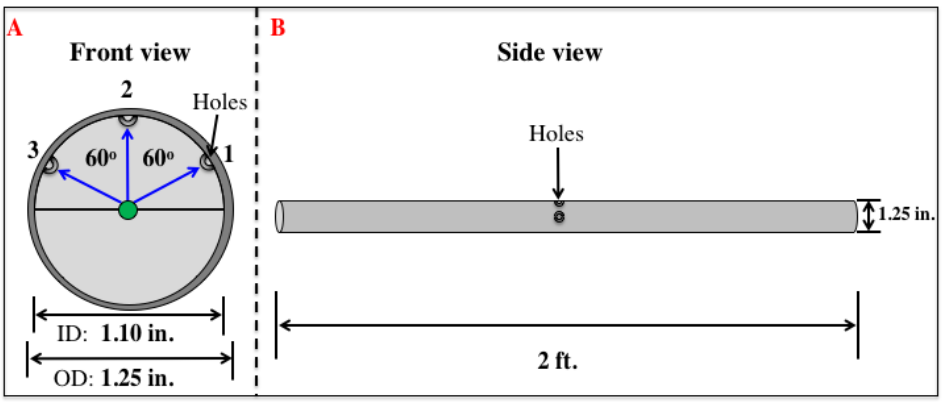

Figure S1: Tube design used to perform volumetric flow rate measurements of the SpinCon II; a) shows the front view of the tube with the description of the holes where measurements were taken with the hotwire anemometer, and b) shows the side view of the tube.

SI.2 Setting FL1- A threshold determination procedure

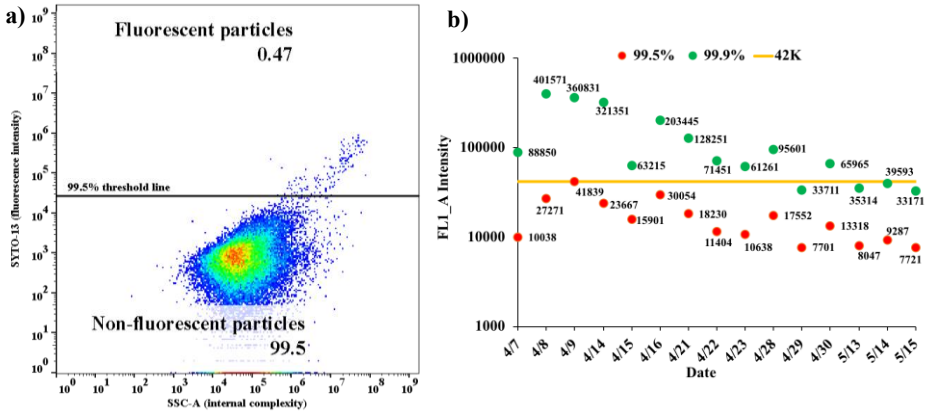

Figure S2: Threshold approach applied to atmospheric samples: (a) April 14, 2015 atmospheric sample blank (no SYTO-13) FL1-A vs. SSC-A plot showing the threshold value (line) to constrain 99.5% of autofluorescent particles (line, FL1_A value: 24k), and (b) summarize the 99.5% and 99.9% calculated values(Y-axis: FL1_A intensity) for each sampling event (x-axis: sampling day in month/day format), and the 42k (41839 units) threshold chosen (yellow line).

SI.3 FCM contour plots and gating

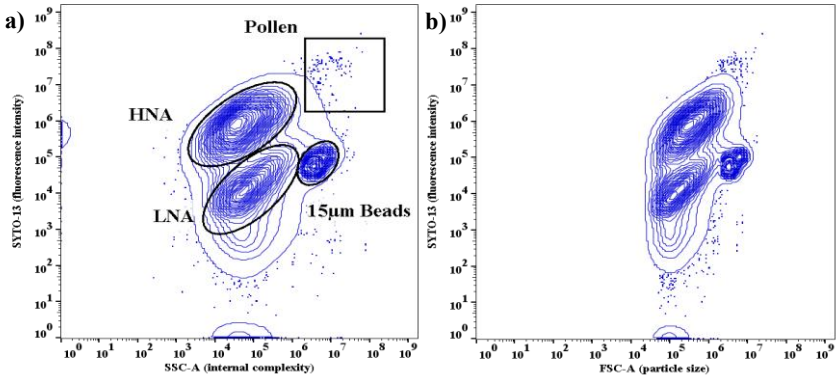

Figure S3: FLI-A vs. SSC-A and FLI-A vs. FSC-A contour plots (example from April 14, 2015 atmospheric sample) used to gate bioaerosol populations using FlowJo maximum resolution (2% contour plots).

SI.4 WIBS-4A sampling losses calculations

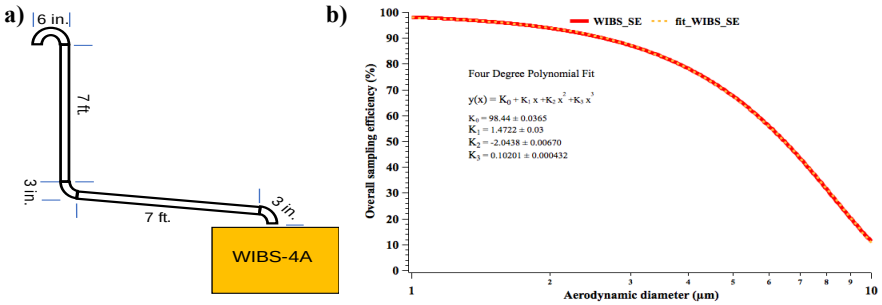

Figure S4: WIBS-4A modeled 15 ft. sampling line in (a) and Particle Losses Calculator overall sampling efficiency results in the 1 to 10 µm size range.

WIBS-4A overall sampling losses for the setup describe in FigureS4a were constrained using the Particle Losses Calculator (PLC) developed by Von der Weiden et al., 2009 calculating the overall sampling efficiency (OSE; aspiration efficiency + transport efficiency). The setup is described as a 5 tubing sections with a 6.35 mm (1/4 in.) inner diameter (ID); 2.3 L min^{-1} flow rate and unit density (1,000 Kg m^{-3}) were also provided as inputs to the model. The output of the model is plotted in Figure S4b (red line) for 1 to 10µm aerodynamic particle sizes. Then, 4hr averaged size distributions were generated for WIBS total particle concentration and all FBAP type categories from 1 to 10µm. The size distributions were generated using as reference the biggest size in each bin (upper bound). For instance, if a particle is between 0.9 µm and 1 µm it will be counted as part of the 1µm bin, and 100 bins were used between 0.1µm and 10µm. Subsequently, a four-degree polynomial regression was applied to the PLC data (Figure S4b) and the equation given by the fit was used to correct WIBS-4A uncorrected size distributions using the midpoint of each bin as the average size to calculate the OSE (e.g. particles in a bin between 1.0 and 1.1 µm will use 1.05µm as the average size to calculate the OSE). In addition, throughout the process of correcting WIBS-4A losses the aerodynamic diameter calculated by PLC is considered equivalent to the optical particle diameter calculated by the WIBS-4A assuming aerosol particles have unit density and understanding that WIBS-4A considers all particles spheres when Mie Scattering approach is applied to calculate aerosol size. The general equation used to correct each bin of the WIBS-4A size distributions is given by:

$$WIBS\ corrected\ \ bin\ (i) = [WIBS\ uncorrected\ bin(i)] * \left[\frac{100}{OSE(i)}\right] \qquad S2$$

where *i* represents each of the size bins in the size distribution (e.g. i=1,2,3…100) and OSE *(i)* is the overall sampling efficiency calculated for each size bin.

SI.5 SEM pictures

1mL of atmospheric sample was filtered through a 0.2µm Nucleopore filter for each sample. The filters were attached to 25mm mounters and coated with a Gold/Carbon sputter. Then, pictures were taken using a LEO 1530 Thermally-Assisted Field Emission (TFE) Scanning Electron Microscope (SEM).

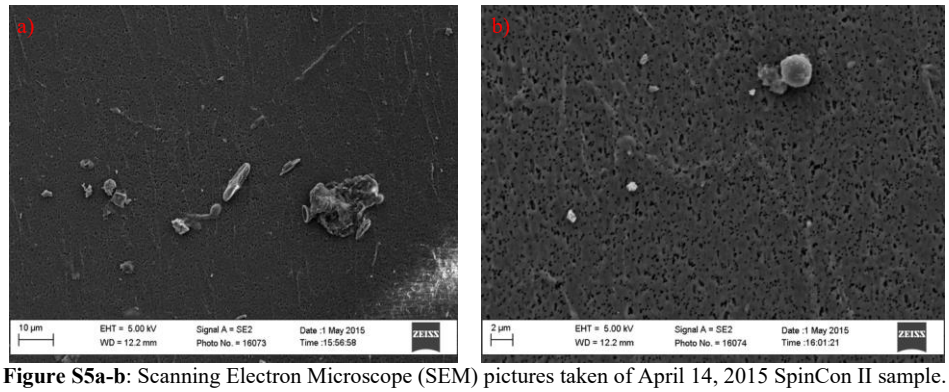

Figure S5a-b: Scanning Electron Microscope (SEM) pictures taken of April 14, 2015 SpinCon II sample. a) shows a heterogeneous population of particles including: dust, bacteria, fungal spores and other particles; b) shows small dust particles and a small fungal spore(~2µm).

SI.6 EPM pictures

Epifluorescence microscopy (EPM) pictures were taken during the design of the FCM protocol. We were able to distinguish different types of particles on them like: bacteria, fungal spores and pollen. Samples were stain using the Live/Dead staining kit. The 1mL stained sample was incubated for 15min; then was filtered in a 0.2µm black Isopore filter and placed in a glass slide. Samples were observed in the Axion Observer D1 epifluorescence microscope (Zeiss). As observed in Figure S6 microorganisms show non-intact cell membranes given the presence of propidium iodide (PI) inside them.

Additional EPM pictures were taken of SpinCon II samples collected in September 9-11, 2015, which are not included in this manuscript, but the same FCM protocol was used as in April-May sampling. During these experiments samples were stained with a 20µg/mL DAPI concentration. The 1mL stained sample was incubated for 15min; then was filtered in a 0.2µm black Isopore filter and placed in a glass slide. Samples were observed in the Axion Observer D1 epifluorescence microscope (Zeiss). Samples show a heterogeneous bioaerosol population as seen in Figure S7a. EPM and FCM results were quantitatively compared in September, 2015 samples. EPM quantification was performed taking 20 pictures (5 rows, 5 pictures by row) of a representative area and it was repeated for a total of 3 representative areas (e.g. bottom, middle and top of the filter) within the filter to have an experimental triplicate. Cells were counted in each representative area and the filtrated volume was used to determine the liquid-based concentration for each sampling event. Thin cells smaller than 5µm were considered bacteria and thick cells between 5-10µm were considered fungal spores. Particles larger than 10µm and irregular-shaped particles were categorized as "others" and they constituted a small fraction of the total cells (~5%). The total PBAP EPM-derived concentrations consisted of the sum of bacteria, fungal spores and "others" particles concentrations. FCM biopopulations identification was performed using the protocol described in Section 3.1 and quantified with the same approach used for the April-May 2015 atmospheric samples (supplemental information, SI.8)

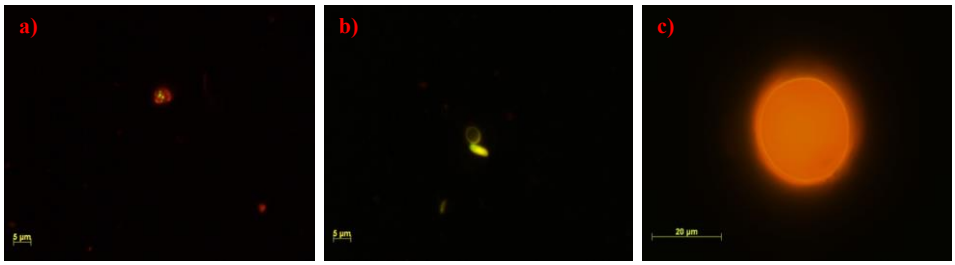

Figure S6a-c: EPM pictures of atmospheric samples collected in March 24, 2015 showing different types of biological particles. a) shows a bacteria agglomerate, b) shows two attached fungal spores and c) shows ~20µm pollen particle.

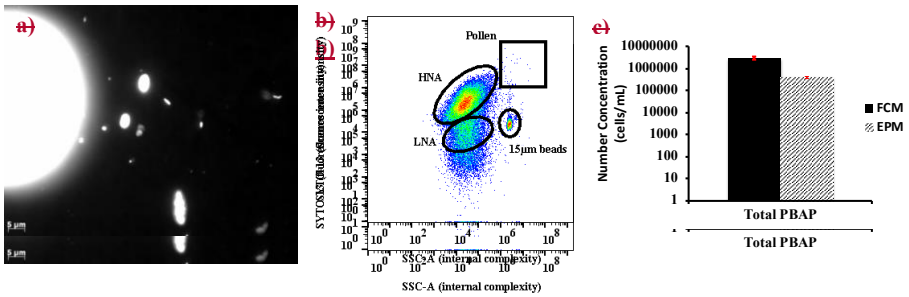

Figure S7a-c: EPM pictures of the September 9, 2015 atmospheric sample (S7a), September 11, 2015 FCM results with identified populations (S7b) and September 11, 2015 EPM and FCM quantitative comparison (S7c).

SI.7 FCM subpopulations particle size determination

The mean size of each population was determined by comparing 1µm, 2µm, 4µm, 6µm, 10µm, 15µm standardize beads (Flow Cytometry calibration kit, Life Technology Inc.) FSC-A scattering distributions with the populations FSC-A scattering distributions. First, standardized beads were analyzed in triplicate by FCM. Then the geometric mean FSC-A intensities were calculated for each bead size (using FlowJo). Two samples were prepared: a) having 10µL of 1µm, 4µm and 10µm beads; and b) having 10µL of 2µm, 6µm and 15µm beads; both diluted to 1mL with Milli-Q water. Samples SSC-A vs. FSC-A plots are shown in Figure S8a-b.

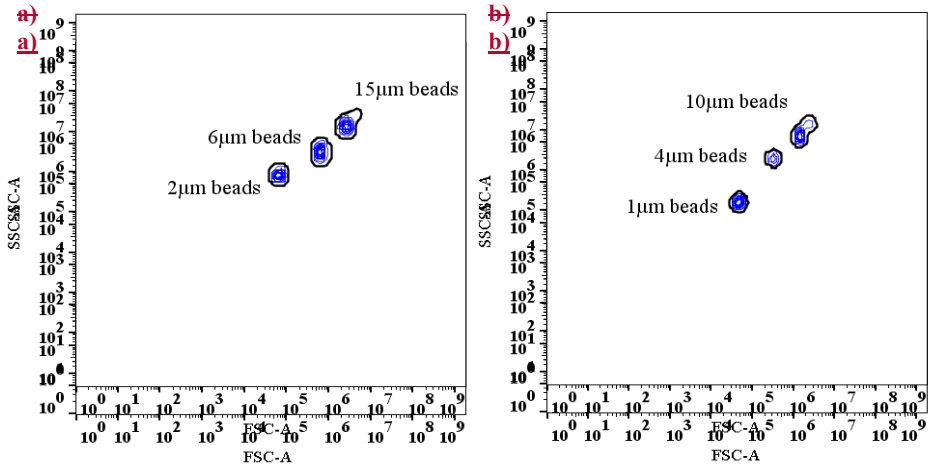

Figure S8a-b: SSC-A vs. FSC-A plots of the FCM calibration beads experiments showing the different type of beads used for size calculations.

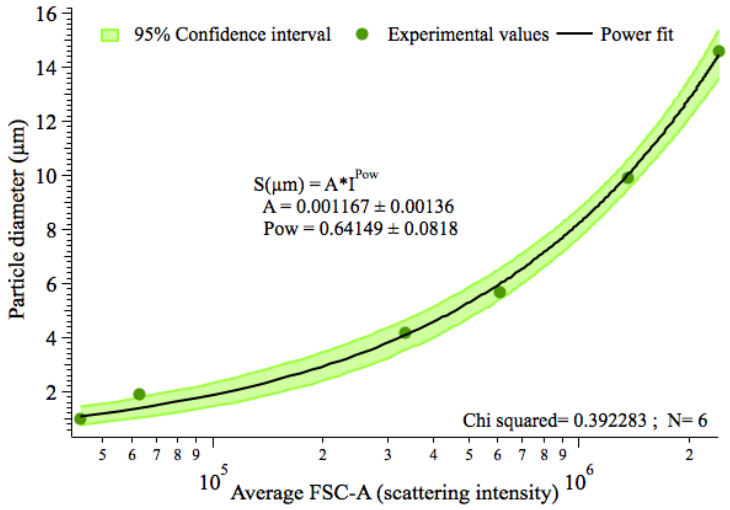

Figure S9: Plot used to determine the subpopulations mean size. Results of the FCM analysis of the calibration beads. X axis is in logarithmic scale.

Then a power regression, shown in Figure S9, was performed to the beads size vs. beads FSC-A fluorescence intensity plot to get an equation to relate beads particle size (diameter) and its respective geometric mean FSC-A intensity.

Based on the regression, the following equation was used to calculate the size of each particle detected by FCM:

$$S(\mu m) = 0.001167\, I^{0.64149} \qquad [S3]$$

where S is the mean size of the particle in µm and I is the averaged geometric mean FSC-A intensity of the particle. The equation calculated the mean size of each particle detected by FCM successfully, but it may have overestimated pollen size given the extrapolation performed to apply the equation to bigger particles (above 15µm diameter). Then, the mean diameter of each FCM population was calculated applying a Gaussian Fit to the geometrically averaged size distributions

generated for all SpinCon II sampling events (Figure S10). Results summarized in Table S1 describe mean sizes of each population during April-May sampling events(n=15)

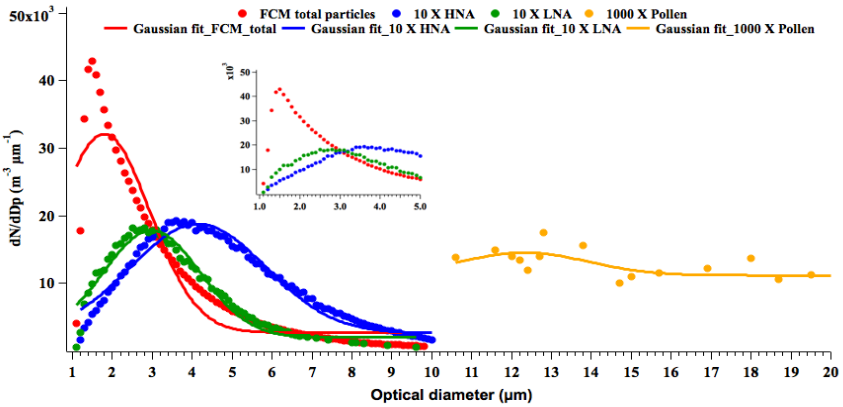

Figure S10: FCM total particles, HNA, LNA and Pollen size distributions (geometric averaged over the 15 SpinCon II sampling events) and Gaussian fits applied to each size distribution to determine the mean diameter of each population.

Table S1: Summary of the mean size (calculated from Gaussian fits in Figure 10) of the FCM total particles and the identified bioparticle populations during SpinCon II sampling events(n=15) . *No collection efficiency (ABC correction factor) applied within this calculation.

	FCM total particles	LNA	HNA	Pollen
Mean diameter (µm)	1.7909	2.9854	4.1506	12.32
Standard deviation (µm)	0.214	0.0638	0.0621	1.67
CV%	12.0%	2.1%	1.5%	13.1%

SI.7 Pollen Autofluorescence

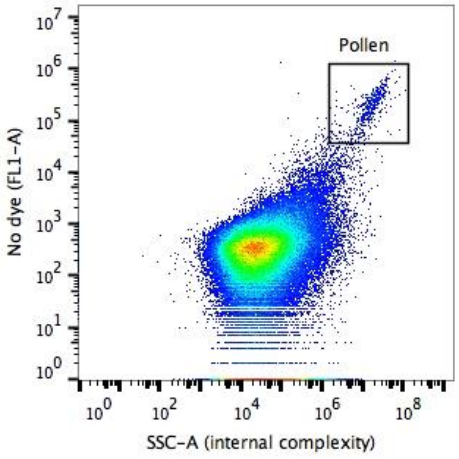

Figure S11: FCM pollen autofluorescence in the atmospheric sample without SYTO-13.

SI.8 FCM PBAP quantification

Equation S4 was used to calculate the liquid-based concentration ($\mathbf{C_{liq}}$) for each FCM-identified bioaerosols population and the total PBAP in the atmospheric and pure culture samples, which is a modification to Lange et al., 1997 quantification equation:

$$\boldsymbol{C_{liq}} = \left(\frac{A * C}{0.99 * B}\right) \quad [S4]$$

where A refers to the population counts above the 42k threshold (41,839 FL1_A units) given by FlowJo, B refers to the volume of the aliquot of sample (mL) used for the FCM analysis and C refers to the inverse of the counting efficiency (ϵ) which is given by:

$$C = \left(\frac{1}{\epsilon}\right) = \left(\frac{beads\ added\ volume \times beads\ original\ concentration}{counts\ given\ by\ flow\ Jo}\right) \quad [S5]$$

The 0.99 factor in equation S4 takes in consideration the 10 µL of 37 wt.% formalin added to the original sample, representing a 1% dilution of the atmospheric sample aliquot. Beads original concentration during these experiments was 2 x 10^7 beads/mL. Then, equation S6 was applied to compute the uncorrected air-based concentration of each population $\mathbf{C_{air}}$:

$$\boldsymbol{C_{air}} = \left(\frac{C_{liq} * D}{E * F}\right) \quad [S6]$$

where *D* refers to the collected sample total volume (mL), *E* refers to the SpinCon II volumetric flow rate (478 L min^{-1} or 0.478 m^3 min^{-1}) and *F* refers to the atmospheric sample sampling time (min).

Finally, the total uncorrected air-based PBAP concentration (m^{-3}) for each sampling event was calculated based on the total particle counts above the 42k threshold value using equations S4, S5, and S6. The quantification of the "unclassified biological" (**UBIO**), biological particles not constrained by gaiting procedure, was performed using the following equation:

$$\boldsymbol{UBIO}\ (m^{-3}) = Total\ PBAP(m^{-3}) - bioLNA(m^{-3}) - HNA(m^{-3}) - Pollen(m^{-3}) \quad [S7]$$

SI.9 HNA and ABC populations correlation

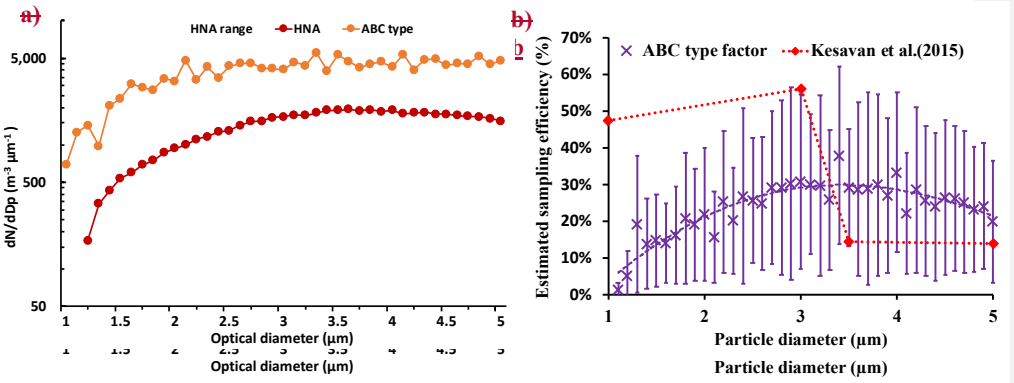

Figure S12: a) FCM HNA and WIBS ABC types 1 to 5µm size distributions (geometrically averaged) comparison including the range (defined by the geometric standard deviation) of HNA

size distributions over the 15 SpinCon II sampling events; b) Estimated sampling efficiency (ECE) comparison to Kesavan et al., 2015 sampling efficiencies for SpinCon I.

FCM correction factors (CF) are based on WIBS-4A ABC type and FCM HNA size distributions in the 1 to 5µm range for each SpinCon II sampling day. CF were calculated for each day the HNA population was identified (n=12) and for the rest of the days (n=3) averaged CF values were used to correct FCM concentrations. FCM size distributions were generated using the same approach used for WIBS-4A (described in SI.4) and FCM particle size was calculated using equation S3. The CF calculations were performed for each bin within the 1 to 5µm range and CF is given by the following equation:

$$CF\ (i) = \left(\frac{\text{ABC corrected bin (i)}}{\text{HNA uncorrected bin (i)}}\right) \quad [S8]$$

where *i* represents each of the bins between 1 to 5µm range in the size distribution. Then, CF for each bin was multiplied by the HNA, ~~bioLNA~~LNA-AT, total PBAP and total particle size distributions to calculate the FCM corrected size distributions. From the corrected size distributions, the number concentration on each bin was acquired and the total corrected concentration in each population constituted the sum of the number concentrations of all bins between 1 to 5µm. In addition, unclassified biological concentrations (UBIO) were calculated using equation S7, but with the FCM corrected concentrations. Finally, the estimated sampling efficiency (ECE) plotted in Figure S12b is given by the following equation:

$$ECE(i) = \frac{100}{CF(i)} \quad [S9]$$

where *i* represents each of the bins between 1 to 5µm range in the size distribution.

SI.10 FCM Pure Cultures experiments

Pure culture experiments were performed during the study as an additional support to the observations seen in the atmospheric samples. Two different types of experiments were conducted: i) the individual microorganisms (bacteria, yeast and pollen) were analyzed to visualize the population of microorganisms; ii) mixtures of the microorganisms were analyzed to understand how they would look all together and see how it compares with what is seen in the atmospheric samples.

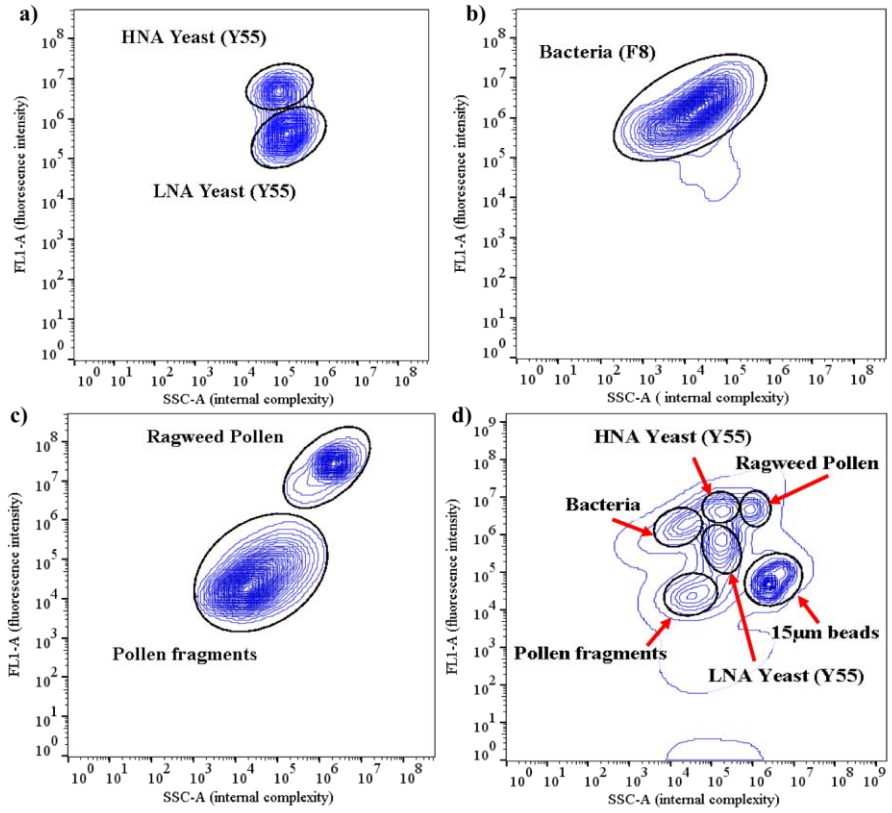

Figure S13: FCM pure culture FL1-A vs. SSC-A plots. a), b) and c) show FCM results of individual yeast isolate (Y55 strain), bacteria atmospheric isolate (F8), and Ragweed pollen, respectively; and d) shows FCM results of the mixture of microorganisms.

Yeast (Y55) and Bacteria (F8) strains used in the experiments were grown overnight in non-limited oxygen conditions. Y55 was grown in 1X yeast extract at 35°C and F8 was grown in 1X LB broth at 30°C. Then an aliquot of each was fixed with formalin. Ragweed pollen (Ambrosia artemisiifolia), purchased to Greer Laboratories (Lenoir, NC), was used without further purification. A 10mg/mL pollen/PBS solution was prepared as working stock. Then different dilutions were performed to yeast, bacteria and pollen samples to reach 10^4-10^5 part. /mL concentration and were individually analyzed by FCM. Figure S13a-c show the results of the individual microbial populations. Then mixtures of the microorganisms were analyzed using the

same SYTO-13 and 15µm beads concentrations used for the atmospheric samples. Results in Figure S13d show populations are close to each other given their similar sizes and internal complexities. Also, microorganism populations show higher SYTO-13 fluorescence intensity than those in the atmospheric samples, as it observed in Figure S13a-d and summarized in Table S2. Among mixed populations experiments we focused in the pollen to pollen fragments ratio given pollen fragments importance in the atmospheric sample bacteria quantification. Based on the results, a 1.1 x 10^4 part. /mL pollen population will release 2.7 x 10^4 part. /mL of pollen fragments when is in contact with aqueous solution, which constitute approximately a 1 to 2.4 ratio (Look Table S2). Given the small pollen concentration seen in the atmospheric samples, it is understood the impact of pollen fragmentation in ~~bioLNA~~LNA-AT quantification will be negligible.

Table S2: Pure cultures triplicate concentrations overview.

PBAP Type	Pure Culture Triplicates			Average (mL^{-1})	Standard Deviation (mL^{-1})	CV (%)
	SC1880	SC1881	SC1882			
Pollen	1.20×10^4	1.04×10^4	1.05×10^4	1.09×10^4	8.96×10^2	8.2%
Pollen Fragments	2.92×10^4	2.27×10^4	2.78×10^4	2.66×10^4	3.41×10^3	12.8%
Bacteria	1.99×10^4	1.75×10^4	1.55×10^4	1.76×10^4	2.23×10^3	12.6%
HNA Yeast	2.61×10^4	2.45×10^4	2.57×10^4	2.54×10^4	8.37×10^2	3.3%
LNA Yeast	4.09×10^4	4.25×10^4	3.65×10^4	4.00×10^4	3.13×10^3	7.8%

Pure culture and atmospheric samples FSC-A, SSC-A and FL-1 properties, summarized in Table S3 and Table S4, show interesting differences in their fluorescence intensities, possibly related to a reduction in the genetic content of atmospheric microorganisms due to starvation.

Table S2: Pure cultures mixture FSC-A, SSC-A and FL1-A properties summary.

PBAP Type	FSC-A Avg.	FSC-A SD	SSC_A Avg.	SSC-A SD	FL1-A	FL1-A SD
Bacteria	7.23×10^4	8.54×10^3	1.52×10^4	2.67×10^3	1.30×10^6	1.81×10^5
HNA yeast	6.03×10^5	1.06×10^4	1.45×10^5	9.44×10^3	4.04×10^6	1.66×10^5
LNA yeast	1.17×10^6	2.29×10^4	1.61×10^5	4.09×10^3	6.16×10^5	1.43×10^5
Pollen	5.03×10^5	9.33×10^4	8.72×10^5	3.94×10^4	4.21×10^6	2.51×10^5
Pollen fragments	7.54×10^4	4.77×10^3	4.27×10^4	1.44×10^4	2.47×10^4	8.46×10^2

Table S3: Atmospheric populations FSC-A, SSC-A and FL-1 properties summary of SpinCon II sampling events (n=15) during April-May, 2015.

	~~bio~~LNA-AT Geo Mean			HNA Geo Mean			Pollen Geo Mean			Beads Geo Mean		
	FSC-A	SSC-A	FL1-A	FSC-A	SSC-A	FL1-A	FSC-A	SSC-A	FL1-A	FSC-A	SSC-A	FL1-A
Average	2.67×10^5	1.40×10^5	7.38×10^4	3.89×10^5	7.87×10^4	6.72×10^5	3.50×10^6	5.88×10^6	6.57×10^6	3.02×10^6	3.28×10^6	5.87×10^4
SD	8.19×10^4	6.91×10^4	1.39×10^4	8.42×10^4	3.00×10^4	2.30×10^5	2.86×10^6	5.85×10^6	2.85×10^6	6.47×10^5	7.73×10^5	4.39×10^4
Max	4.52×10^5	2.71×10^5	1.00×10^5	4.84×10^5	1.08×10^5	1.08×10^6	1.32×10^7	2.62×10^7	1.35×10^7	3.95×10^6	4.59×10^6	1.80×10^5
Min	1.36×10^5	4.71×10^4	5.19×10^4	1.99×10^5	2.48×10^4	3.11×10^5	1.68×10^6	2.73×10^6	2.87×10^6	1.69×10^6	1.85×10^6	1.46×10^4

SI.11 Arizona Test Dust (ATD) FCM Experiments

Experiment using unprocessed and commercially available (Powder Technologies Inc.) Arizona Test Dust (ATD) were conducted by suspending ATD in 1X PBS. 20mg of the ATD were diluted into 10mL of PBS and fixed with 1 vol.% formalin overnight. Then, a 1/20 dilution of the initial ATD solution was filtered through a sterile 10µm pore size Isopore filter (Millipore Sigma) to prevent clogging the flow cytometer with big particles. Subsequently, ATD was stained with 2.5 µM SYTO-13 (same concentration used to stain the atmospheric samples) and incubated in the dark at room temperature for 15 min. before been analyzed by Flow Cytometry. Histograms of the analyzed ATD solutions (~10^6 particles mL^{-1}) below show the fluorescence intensity (FL1-A intensity) distributions of unstained (Figure S14a, blue) and stained ATD (Figure S14b, orange) particles are negligibly different, and 100% of the stained ATD particles have a FL1_A intensity below the threshold value (41,839) used to distinguish between abiotic and biotic particles. ATD results support SYTO-13 does not bind to abiotic particles and agree the applied fluorescence threshold effectively filters out abiotic particles.

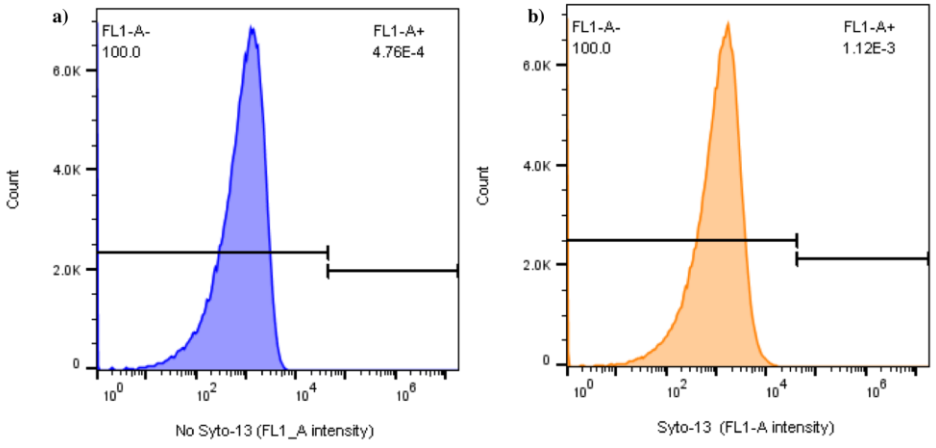

Figure S14: ATD FL1_A intensity histogram distributions for unstained (a) and (b) stained ATD, where FL1_A- and FL1_A+ subpopulations represent the percentage of particles with FL1_A intensity above and below the fluorescence intensity threshold value (41,839), respectively.

SI.12 FCM plots for SpinCon II sampling events

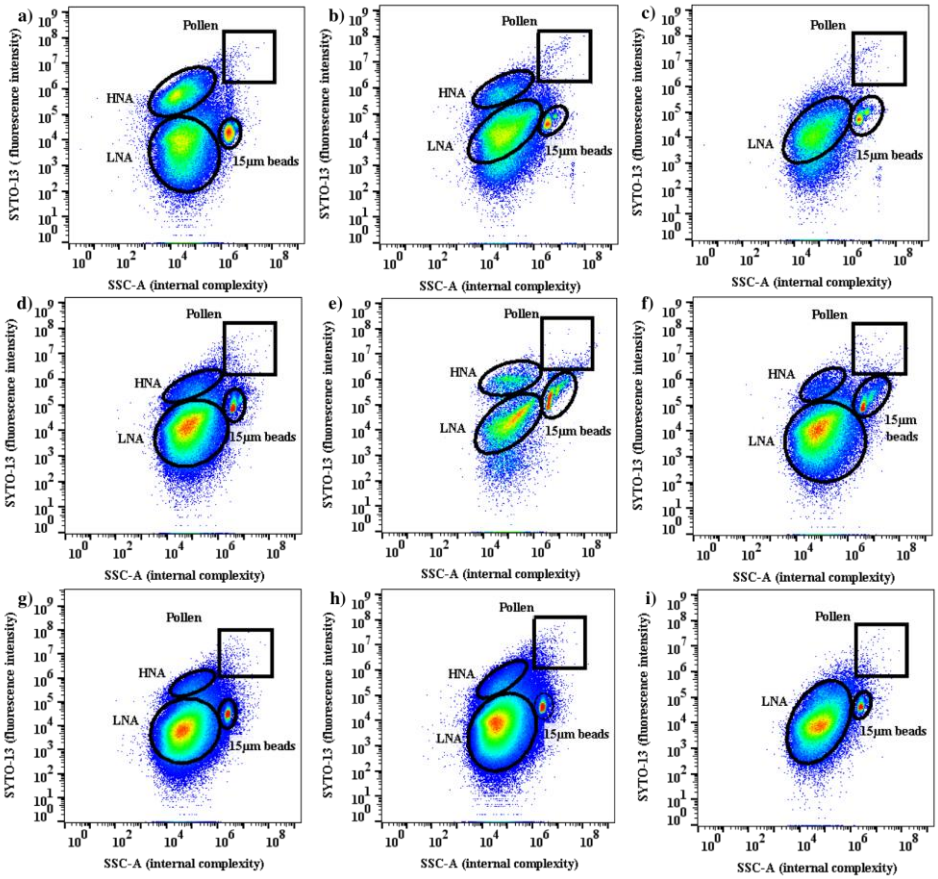

Figure S15a-i: FCM FL1-A vs. SSC-A plots (pseudo-color plots show higher particle accumulation in green to red regions) for the following 2015 April-May SpinCon II sampling events: a) April 7, b) April 8, c) April 9, d) April 28, e) April 29, f) April 30, g) May 13, h) May 14 and i) May 15.

SI. 13 1.0µm polystyrene beads cutoff test

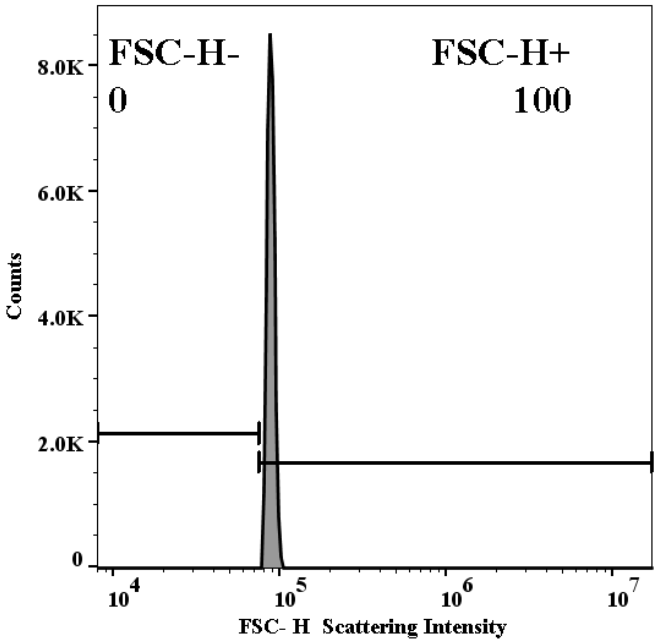

Figure S16: 1.0µm polystyrene beads histogram showing the totality of them have FSC-H scattering intensities above the 80,000 units. Experiment performed using the FSC-H default threshold and concentrations agree to that provided by the manufacturer.

SI. 14 WIBS total particle concentration vs. FBAP types correlation

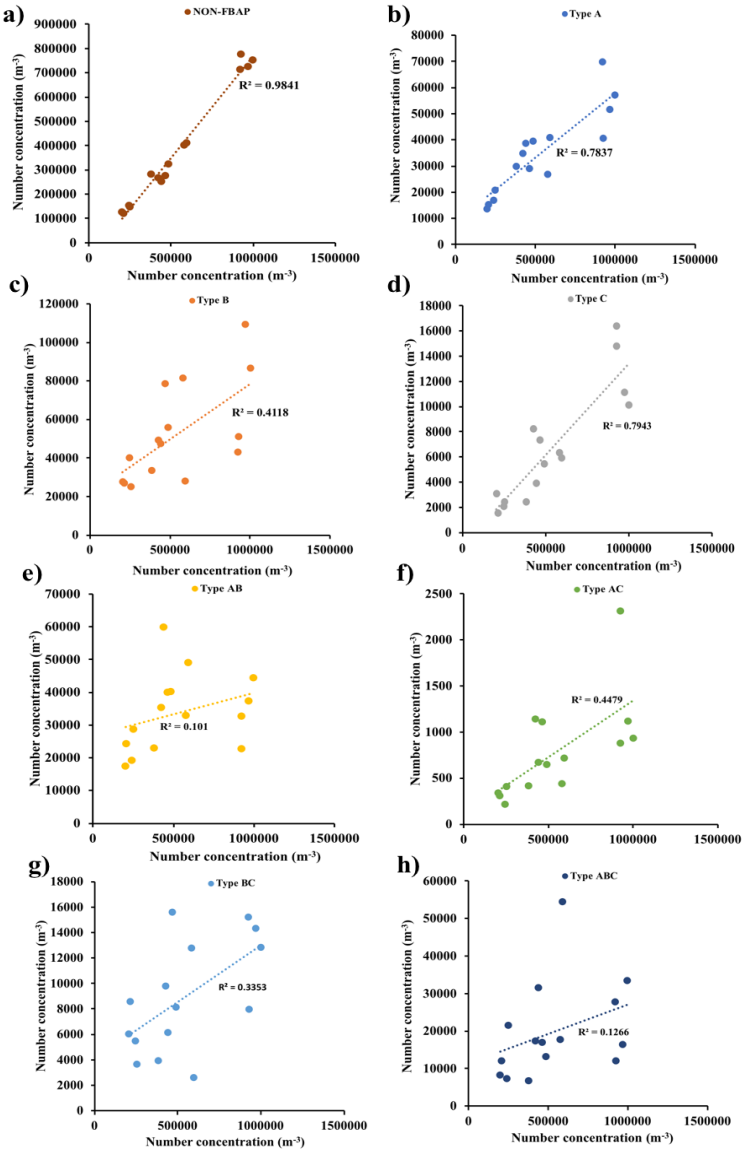

Figure S17: 4h averaged WIBS total particle concentration comparison to FBAP types concentration including: a) NON-FBAP, b) Type A, c) Type B, d) Type C, e) Type AB , f) Type AC, g) Type BC and h) Type ABC.

SI. 15 WIBS corrected, FCM uncorrected and FCM corrected total concentration variability

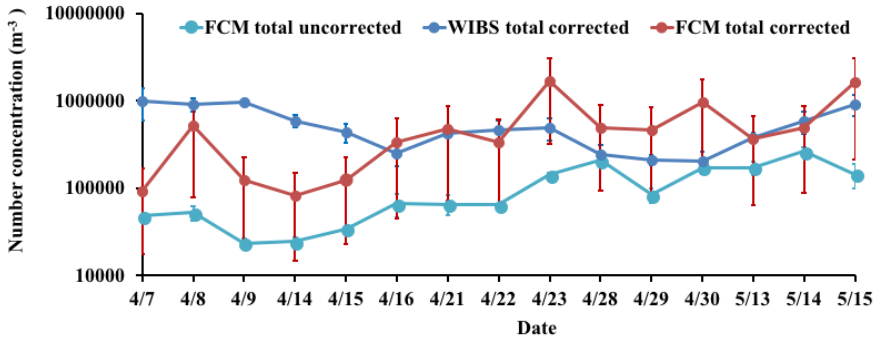

Figure S18: WIBS corrected total particle concentration (4 hr. avg.), FCM uncorrected concentration and FCM corrected (using ABC size distributions) concentration variability between April 7 to May 15, 2015

SI.16 Type B and ~~bioLNA~~LNA-AT anticorrelation

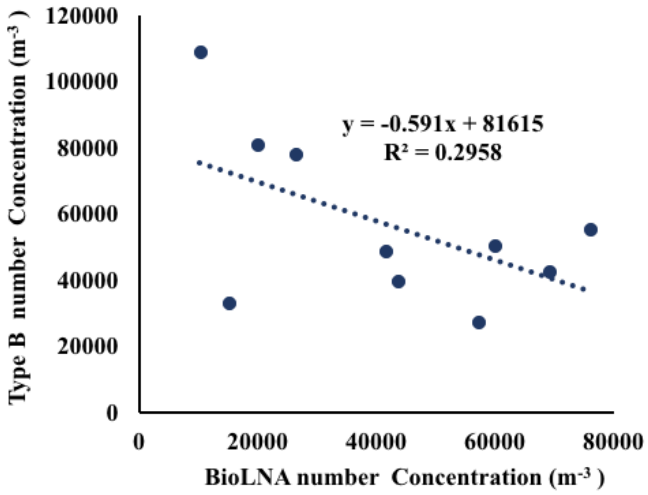

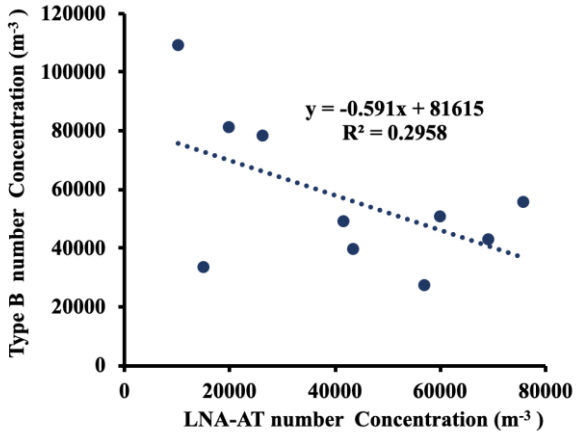

Figure S19: Type B and ~~bioLNA~~LNA-AT number concentration anti-correlation on dry days (n=10)

Formatted: Font: Bold

SI. 17 WIBS total particle vs. Jefferson St. PM10 mass

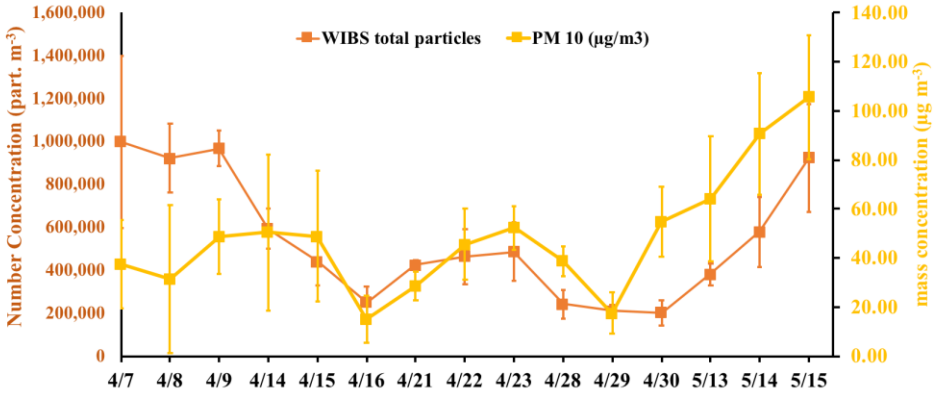

Figure S20: 4h averaged WIBS total particle concentration (left Y axis) and PM_{10} mass concentration (right Y axis) for each SpinCon II sampling event.

459

SI.18 Meteorological Data

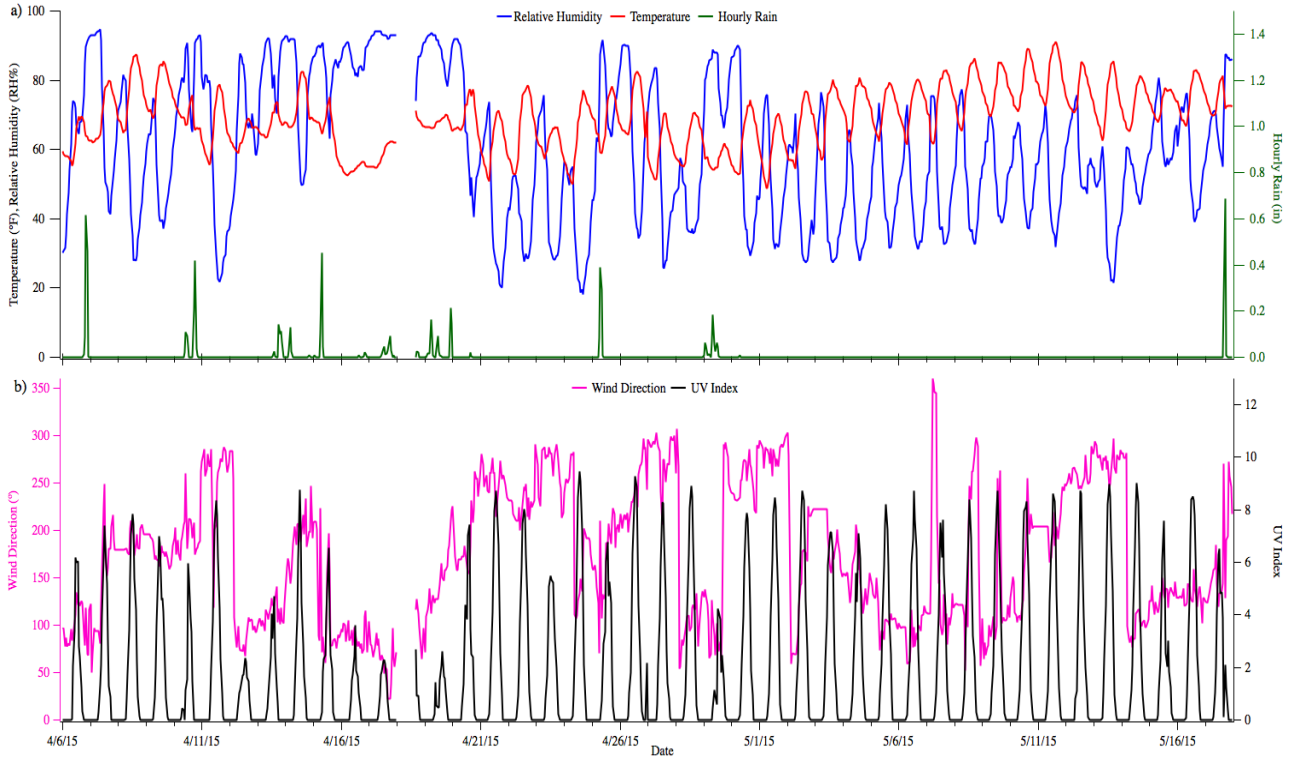

Figure S21: April-May meteorological data summary (hourly averages). Includes relative humidity, temperature, hourly rain, wind direction and UV index

SI.19 Pollen and LNA number concentrations comparison

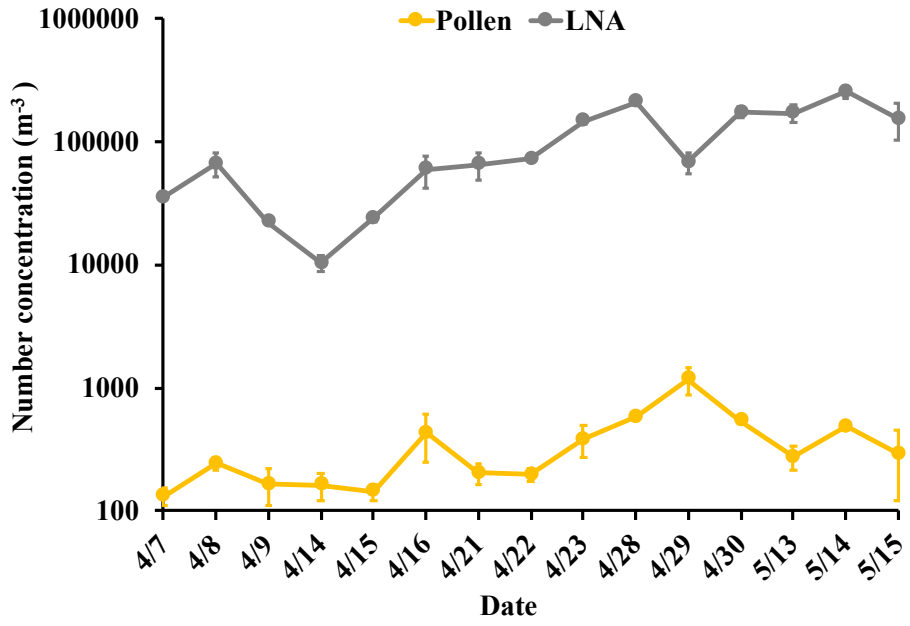

Figure S22: Uncorrected LNA and pollen population number concentrations throughout SpinCon II sampling events.

SI.20 WIBS-3 and WIBS-4 FBAP Quantification, and Perring et al. 2015 Approach

WIBS-3 and WIBS-4 models have been actively studied to determine which channel best detect bioaerosols and to cluster different types of PBAP (Robinson et al., 2013; Crawford et al., 2014; Gabey et al., 2010). Both models use filtered xenon flash lamps to excite particles at 280nm and 370nm wavelengths and detect PBAP autofluorescence in two regimes (For WIBS-3, FL1: 320-600nm and FL2: 410-600nm; For WIBS4, FL1: 310-400nm and FL2; 420-650nm). Three separate fluorescence channels for each model: (i) channel A: detection in FL1 following 280nm excitation, (ii) channel B: detection in FL2 following 280nm excitation and (iii) channel C: detection in FL2 following 370 nm excitation, are then available for FBAP determination. The main difference between WIBS models is that the fluorescence detection regimes overlap in channels A and B for the WIBS-3, but not for the WIBS-4. WIBS-3 FBAP quantification cannot be compared directly with WIBS-4 due to channel A and B overlap, but FBAP detection in all

channels have been consistent between both models (Robinson et al., 2013). WIBS-4 contains two switchable gain settings (e.g. high gain (HG), low gain (LG)), allowing it to measure 0.5µm to 12µm particles in HG and 3µm to 31µm particles in LG setting. On the other hand, the second generation of the WIBS-4, named WIBS-4A, maintains single gain settings and evaluates particles between 0.5µm and 20µm (Fennelly et al., 2017).

Gabey et al. (2011) concluded, using a WIBS-3, that channel C was most efficient in quantifying FBAP either in the Borneo tropical forest or in the urban environment of Manchester, UK. Healy et al. (2014) found higher channel A FBAP concentration in Killarney, Ireland using WIBS-4. Pure culture experiments with WIBS-4 have shown high detection efficiency of channel A toward *Pseudomona syringae* bacteria (Tropak et al., 2013). Hernandez et al. (2016) used WIBS-4 to test the intrinsic fluorescence fingerprints of 29 fungi, 13 pollen and 15 bacteria species and suggested channel A is most suitable for discriminating bacteria and fungi, channel C is most suitable for pollen and channel B can be influenced by abiotic particles. In addition, among FBAP categories (Perring et al., 2015) bacteria is mainly detected as type A, fungal spores shown multiple fluorescence types (e.g. A, AB, BC and ABC) and pollen is mainly detected as type BC and ABC. However, PBAP detection effectiveness by specific channels varies considerably between instruments, which suggests a thorough calibration may be necessary. Furthermore, Savage et al. (2017) used WIBS-4A to show FBAP fluorescence also varies with particle size, especially for pollen and fungal spores and proposed pathways of change by which particles may transition from type A or type B to type ABC as they increase size. FBAP type variation with particle size is important to consider as the approach of Perring et al. (2015) is used to better understand what FBAP type is best detected (e.g. bacteria, fungal spores, pollen).

Several studies have used the Perring et al. (2015) FBAP categories to characterize PBAP in multiple environments across the globe (Yue et al., 2017; Gosselin et al. 2016; Yu et al., 2016). Perring et al. (2015), using a WIBS-4, studied atmospheric PBAP onboard a Skyship 600 aircraft operating between 300m and 1km above ground level at 10 geographic regions across the United States; the study concluded that type AB (~30%) and ABC (~25%) is the most abundant of FBAP particles in the Southeastern US (East Texas to Central Florida), and AB (~1.9 µm) and ABC (~2.6 µm) median sizes are characteristic of mold spores (fungal spores of unknown amount of species predominant on humid and warm environments; www.cdc.gov). In addition, FBAP concentrations in the Southeastern US range from 2×10^4 to 8×10^4 m^{-3}, constituting 3-24% of the total supermicron

particle number between 1 and 10µm diameter. In the Southwestern US, Perring et al. (2015) shows AB and ABC types contribute less due to a higher relative contribution by types B (~25%), BC (~20%) and C (~5%), and total FBAP constitute 5-10% of the total supermicron particles. Furthermore, Perring et al. (2015) found the concentration of ABC type PBAP on the surface and aloft did not vary throughout the Southeastern US. In the highly vegetated Rocky Mountains Gosselin et al. (2016) found (using a WIBS-3) that ABC type particles always are a significant fraction of FBAP (at least 20%) and are especially enhanced during rainy days (during or post-rain events) to ~ 65% of the total FBAP, owing to the release of wet-ejected fungal spores following precipitation (Huffman et al., 2013). However, during dry days, types BC and C increase their relative fraction to ~30% and ~40%, respectively (Perring et al., 2015). Limited studies have looked closely at the FBAP categories in urban environments. In Nanjing, China, Yu et al. (2016) observed that types B (~45%), BC (~25%) and C (~15%) dominate the FBAP concentrations during autumn. All FBAP types, except type C, correlated with black carbon and $PM_{0.8}$ concentrations (particle mass with diameter below 0.8µm), suggesting a strong interference by combustion sources; Type C PBAP ($6.6 \times 10^5 \pm 5.5\times 10^5$ m^{-3}) was considered more representative of bioaerosols, although with unknown interference from abiotic particles. Similarly, Yue et al. (2017) found a dominance of type B PBAP (~66% of total FBAP) during clean and polluted events in wintertime Beijing, China; interestingly, the FBAP contribution to the total particle concentration is higher during polluted events (13-24%) than during clean events (12-14%). FL1 type particles (sum of types AC, ABC, AB and A) are more abundant in clean periods (~25%) than in polluted periods (10.1%), while the fraction of type C FBAP is higher during polluted periods (~20%) than during clean periods (~5%).